Electrically Assisted Vat Photopolymerization 3D Printing of Bioinspired Hierarchical Structures with Controllable Roughness for Hydrophobicity Enhancement

by

Gana Sai Kiran Avinash Raj Dwarampudi

A Thesis Presented in Partial Fulfillment
of the Requirement for the Degree
Master of Science

Approved November 2022 by the
Graduate Supervisory Committee:

Xiangjia Li, Chair
Kailong Jin,
Leila Ladani

ARIZONA STATE UNIVERSITY

December 2022

ABSTRACT

Biomimetics is a field where natural and biological systems are replicated in a lab. The evolved hierarchical designs of the floating leaves of the water fern Salvinia Molesta are taken as inspiration as they reveal excellent dual scale roughness capability which also presents superhydrophobic properties in the nature. The microscale eggbeater-shaped hairs are coated with microscopic granules and nanoscopic wax crystals (dual-scale roughness) and wrinkled hydrophilic patches are coated with wax crystals which are evenly distributed on the terminal of each hair. The combination of features with diverse wettability, such as wrinkled hydrophilic patches atop superhydrophobic eggbeater hairs, makes such structures unique. The hydrophilic patches bind the air-water interface to the tips of the eggbeater hairs and inhibit air bubble formation. Salvinia effect of several Salvinia species has been extensively researched. Superhydrophobicity is attracting increasing attention for various applications. Salvinia exhibit multiscale roughness because of the unique combination of smooth hydrophilic patches on elastic eggbeater structures decorated with nanoscopic wax crystals. However, how to reproduce such hierarchical structures with controllable surface roughness is challenging for current fabrication approaches, which hinders the applications of these superhydrophobic properties as well as multi-scale roughness on surfaces in engineered products.

The objective of this research is to fabricate and study the superhydrophobic structures using electrically assisted Vat Photopolymerization. In this project, an electrically assisted Vat Photopolymerization 3D printing (e-VPP-3DP) process was developed to control the surface roughness of printed eggbeater structures with distribution of multi walled carbon nanotubes (MWCNTs) for multi scale roughness. Vat

Photopolymerization (VPP) is a Photopolymerization technique where a Photo Curable resin is used to rapidly produce dense photopolymer parts. A fundamental understanding of e-VPP technique to create superhydrophobic structures was studied to identify the relation between geometric morphology and mechanical enhancements of these structures. The correlation between the material properties for different weight percentage mixtures of MWCNT, printing parameters and the mechanical properties like attaching forces, surface roughness and superhydrophobic nature are also identified with this study on bioinspired hierarchical structures.

ACKNOWLEDGMENTS

I want to start by expressing my heartfelt and sincere thanks to my advisor, Professor Xiangjia Li, for providing me the chance to serve as a Research Aide in the Lab of Manufacturing Innovations and for the support, direction, and encouragement she provided me with over the duration of my thesis research. Thank you for spending a lot of time with me over the course of the last two academic semesters, giving me advice on how to handle various situations and supporting my quest for knowledge with unending patience and leadership. I also want to express my profound gratitude to the members of my committee, Professors Kailong Jin and Leila Ladani.

I'd want to express my appreciation and gratitude to Tengteng Tang, my lab mate, for providing me with all the assistance I required, as well as original suggestions for my work and unwavering support all during my research. As a graduate service assistant and teaching assistant for Professor Kangping Chen's class, I must also express my gratitude to him. I have the chance to improve my presentation and teaching skills.

Finally, I want to thank everyone in my family and group of friends for their love, support, and encouragement over the years, especially during my graduate studies. In addition, I want to express my gratitude to all of my lab mates, colleagues, mentors, and advisors for their unwavering support and assistance during my degree.

TABLE OF CONTENTS

Page

CHAPTER Page

LIST OF FIGURES

Figure Page

Figure Page

Figure Page

LIST OF EQUATIONS

Equation Page

CHAPTER 1

INTRODUCTION

1.1 Biological Superhydrophobic Structures

The design of the next generation of superhydrophobic surfaces are inspired by biological architectures that utilizes uniquely evolved hierarchical structures [1-9]. Numerous aquatic and semiaquatic species had developed advanced structures that can maintain a stable air layer underwater for extended periods of time, either for insulation or breathing [10-14]. For instance, the developed hierarchical structures of the floating leaves of the water fern Salvinia Molesta exhibit superior long-term air-retention capabilities, especially in a turbulent flow environment [14-26]. Such complex surface designs comprise of eggbeater-shaped microscale hairs embellished with nanoscale wax crystals and tiny granules (dual-scale roughness) and wrinkled hydrophilic patches lacking wax crystals are uniformly distributed on the terminal of each hair (Figure 1) [14-16]. The combination of features with various wettabilities, such as wrinkled hydrophilic patches atop superhydrophobic eggbeater hairs, gives such formations their distinctiveness. The hydrophilic patches sustain air layers even in turbulence and low-pressure circumstances by pinning the air-water interface to the ends of eggbeater hairs and preventing air bubble formation and separation (the "Salvinia Effect") [21]. Different Salvinia species' Salvinia effects have been extensively examined, and it has been found that a variety of hair structure geometries are efficient at keeping air over the long term [22]. The air layer underneath the fluctuations is readily broken by the formation of air

bubbles, but the hydrophilic patches can considerably raise the activation energy by pinching the air-water interface [22].

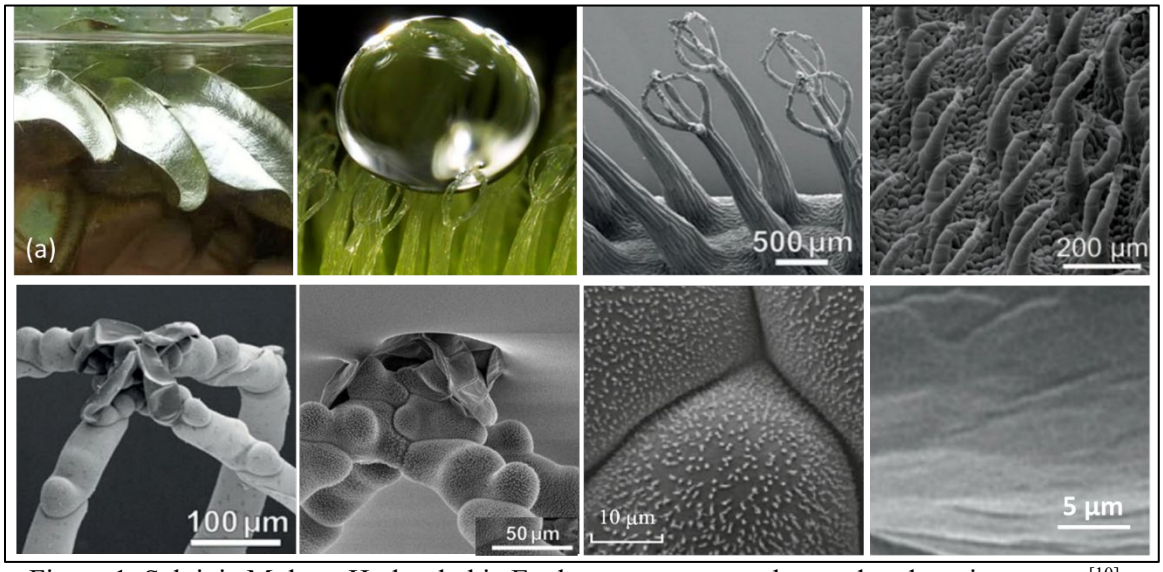

Figure 1: Salvinia Molesta Hydrophobic Eggbeater structures observed under microscope [10].

The superhydrophobicity phenomenon is the explanation of this wettability behavior. Superhydrophobicity is the scientific term for a highly water-repellent disposition. Superhydrophobicity often refers to the measurement of a water drop's contact angle at the liquid/solid interface. A solid surface's wettability is a property that is influenced by surface shape and chemical composition. A drop with a spherical shape is created when a liquid drop strikes a surface. The spherical drop and the surface have a noticeable contact angle at the circular solid-liquid-vapor contact line.

1.2 Traditional Manufacturing of Superhydrophobic Structures

To create superhydrophobic structures, controlling surface topology and roughness is crucial. Various methods of creating various kinds of superhydrophobic structures inspired by nature, like Salvinia, have been published in recent literature. Since wettability is a crucial factor in the formation of hydrophobic surfaces and needs to be

regulated, it is important to identify and manage the motivating factor to produce an ideal superhydrophobic surface. In order to construct superhydrophobic structures using conventional techniques like modeling, laser, coating, etc., several types of studies have been conducted. For instance, traditional terry fabrics with hydrophobic treatments and nylon flock layers with electrostatic flocking were investigated for potential use in overwater life-saving equipment to mimic the long-term air-retaining capabilities of the Salvinia leaf [29,30]. However, the trapped air layers can only operate in static, low-pressure environments. The surface textures were altered to become hydrophobic using glass nano-coating [41], chemical vapor deposition (CVD), femtosecond laser texturing [38], and plasma nanotexturing [39], Electrochemical Etching methods [40].

Some of the traditional manufacturing methods that are popular for coating the surfaces with nano fillers are Electrodeposition of metal ions (Figure 2a) on the surface and also Electrochemical etching (Figure 2b). The scanning electrodeposition approach (Figure 2c), in general, is a flexible, controlled, easy, and quick method for creating coatings with outstanding superhydrophobic characteristics. It is an environmentally benign technique of manufacture since it does away with the need for chemical modification, which further does away with any potential environmental impacts [41]. Whereas the other traditional manufacturing techniques like Laser Ablation (Figure 2d) focus more on the mechanical properties of these structures like corrosion resistance, anti-abrasion than the structural integrity of the structures.

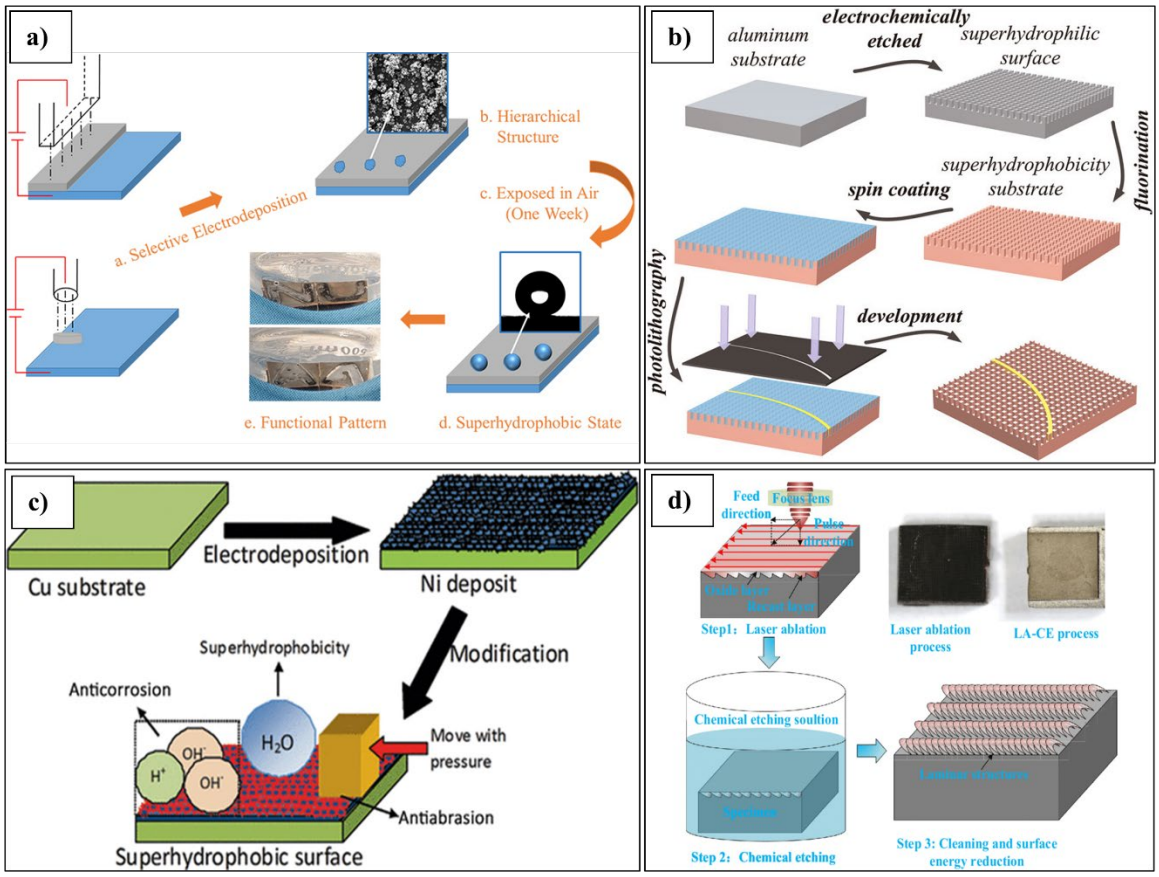

Figure 2: a) Electrodeposition of metal ions Technique [41]; b) Electrochemical Etching and Photolithography Technique [42]; c) Ni electrodeposition for Superhydrophobic Anti-abrasion Technique [43]; d) Laser Ablation Chemical Etching [44].

1.3 Additive Manufacturing and Advantages

The term "additive manufacturing" (AM) refers to a group of modern manufacturing techniques used to create three-dimensional prototypes from CAD models. These processes incorporate and link materials in layers to create structures, which is a feature of every one of them. These methods are also known as layered manufacturing methods. While comprehensive 3D models are employed in the AM process, traditional procedures use 2D models. This CAD-generated 3D geometric data is separated into layer data, and the computers are used to directly create the layers. Some of the examples of AM are Material Extrusion, Powder bed fusion, Binder jetting, Direct Energy Deposition,

Stereolithography, Vat Photopolymerization. Selective laser sintering (Figure 3a) is an additive manufacturing process that employs a laser as the energy and heat source to melt powdered material together to form a solid structure. The laser is automatically directed to locations in space specified by a 3D model. With Direk Ink Writing (DIW) (Figure 3b), materials are deposited layer by layer as the print head is continuously raised to produce a three-dimensional structure. The substance is transformed into pellets or a paste. A crucial parameter is the melting point of the pellets or the viscosity of the paste [54].

The following are the advantages of using AM technologies over traditional manufacturing techniques:

- Form, fit, and function testing may be performed considerably earlier in the design cycle using a physical model that can be quickly produced from CAD drawings.
- Design to prototype iterations are completed more quickly and errors resulting from improper design interpretation are eliminated.
- A prototype may be created from a CAD model without the assistance of a qualified machinist, fixture designer, or NC coder.
- Applications for Core/Cavity include die-casting, investment casting, and plastic molding.
- Depending on the technique utilized, some of the pieces created may be used as patterns for investment or sand casting in addition to manufacturing plastic prototype models directly.

- A longer lead time is necessary for creating dies and molds. Tooling may be created faster thanks to AM technology. These speeds up the process of getting items to market.
- With the right materials, the model may be used in the subsequent assembly steps to produce the finished pieces. Additionally, it is a manufacturing technique.

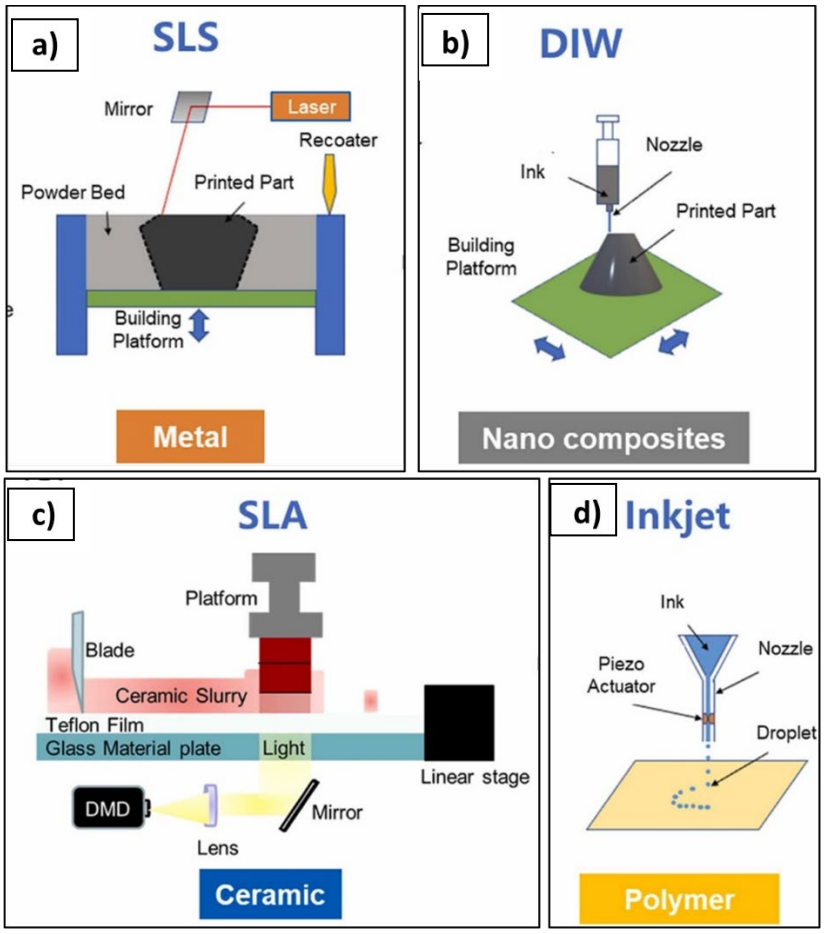

Figure 3: a) Selective Laser Sintering (SLS); b) Digital ink Writing (DIW); c) Stereolithography 3D Printing (SLA); d) Inkjet 3D Printing [54].

Some of the popular AM Techniques are shown in the Figure 3. Stereolithography (Figure3c) is a technique that works by employing a strong laser to build the required 3D form by hardening liquid resin that is kept in a reservoir. The layer-by-layer deposition

method used in 3D inkjet printing (Figure 3d) is comparable to other 3D printing methods. A 3D mechanical model of the product is utilized to produce printing instructions for each layer, exactly as with popular fused deposition modeling (FDM) systems.

Vat Photopolymerization: In Vat Photopolymerization [2] (Figure 4), a photopolymer resin is used to create/print the structures. A photopolymer, also known as light-activated resin, is a kind of polymer that alters the way its molecules behave when it is subjected to light, typically light that is in the ultraviolet or visible range of the electromagnetic spectrum. All kinds of vat photopolymerization printers employ special resins called photopolymers as the printing medium. A process known as photopolymerization causes the molecules of liquid photopolymers to quickly bond together and cure into a solid state when exposed to specific wavelengths of light. The build platform is typically partly buried at the liquid's surface in the majority of 3D printers that use vat photopolymerization. Using models from a CAD file, the printer controls a light source to selectively cure the liquid photopolymer into a solid layer. The procedure is then repeated for the successive layers, down till the full design is formed, submerging the construction platform again in the resin that's been previously utilized. Vat photopolymerization method is used in stereolithography (SLA), the first patented and commercially available AM process.

There are different types of Vat Polymerization Techniques. Some of them are Stereolithography, Digital light Processing and Continuous Digital Light Processing. Vat polymerization techniques are effective for producing items with a clean surface finish and fine details. Consequently, they are ideal for a range of dental and medical

applications, reduced experimental injection molding, and jewelry. One of the major limitations of vat polymerization is the brittleness of the components that are produced.

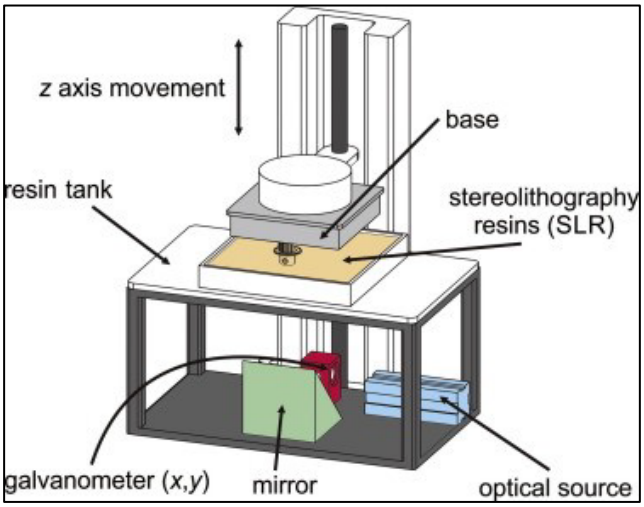

Figure 4: Vat Photopolymerization Technique CAD Model [21]

1.4 Motivation and Objectives

To develop biomimetic superhydrophobic surfaces with multi-scale roughness for underwater applications, such as low friction fluid transfer and drag reduction, the "Salvinia Effect" offers a novel approach. However, current fabrication techniques find it difficult to create bioinspired hierarchical structures made of microscale superhydrophobic hair with dual-scale roughness and wrinkled hydrophilic patches to replicate the "Salvinia effect," which limits the use of such biomimetic architecture in engineered products. Conventional methods like deposition and sputtering may be used to create superhydrophobic, two-dimensional (2D) surfaces with nanoscale roughness that are inspired by biological surfaces. However, the fabrication methods have a restriction on the precise control of roughness and wettability for various three-dimensional (3D) intricate structure sections; as a result, the manufactured structures still have a poor air

retention performance. Therefore, a key problem for 3D printing of bioinspired superhydrophobic materials is how to precisely regulate surface roughness and wettability.

Compared with traditional manufacturing processes, 3D printing can print better bioinspired structures because: By creating parts layer by layer, AM makes effective use of raw materials as opposed to traditional subtractive manufacturing, which requires significant amounts of material to be eliminated. Frequently, reusing leftover materials just requires little processing. In addition to the primary machine tool, traditional manufacturing processes need for auxiliary materials including fixtures, jigs, cutting tools, and coolants. No more resources are needed for AM. Therefore, components may be produced locally by small businesses. This offers a chance to enhance supply chain dynamics. Parts with complicated features may be produced in a single piece since there are no tooling restrictions. In other words, it is unnecessary to forgo a part's functioning in favor of manufacturing simplicity. Additionally, it is feasible to construct a single component with a range of mechanical characteristics (flexible in one part and stiffer in another part). This creates chances for innovative design. AM machines are affordable in small batch manufacturing since they don't need expensive setups. Rather than operator expertise, the process determines the quality of the products. As a result, it is simple to coordinate production with client demand. Because complicated components are manufactured in separate pieces, the issues of line balance and manufacturing bottlenecks are essentially removed.

The objective of this research is to use Vat Photopolymerization 3D printing process to fabricate and study the superhydrophobic eggbeater structures inspired from

Salvinia Molesta and their mechanical properties like surface roughness and attaching force and compare them to identify the correlation between the geometric morphologies where different distances/gaps between each individual eggbeater structure are designed and material selections where the prints are made with 0.5%, 1%, 1.5%, 2% and 2.5% MWCNT weight percentages added to the photopolymer resin with these mechanical properties. Comparing these outputs makes it possible to determine the best possible design for these structures to solve the challenges to achieve better superhydrophobicity, dual-scale surface roughness properties as well as the development of a novel AM technique for multiple applications.

CHAPTER 2

LITERATURE REVIEW

2.1 3D Printing of Superhydrophobic Structures

2.1.1 3D printing of structures with Superamphiphobicity

Surfaces with contact angles larger than 150° and low contact angle hysteresis (CAH) not just for probing water but also for low-surface-tension "oils" are said to be superamphiphobitic as a result of the interaction between surface roughness and surface chemistry [45]. All the bio-inspired eggbeater constructions only have one layer that functions in contact with liquid. In this procedure, a Br-containing vinyl-terminated initiator for surface-initiated atomic transfer radical polymerization is added to the printing ink. With the Br spread (Figure 5a) both within and on the surface of 3D printed objects, the mixed resin may create highly cross-linked networks during the 3D printing process. The outermost Br of a 3D-printed object then enables post-surface modification to create any kind of polymer brush using SI-ATRP [24]. Surface modification using various polymer brushes may provide a variety of surface properties, including superhydrophobicity (Figure5b) and superhydrophilicity, as well as biocompatibility, antibacterial properties, and even metallization. As a result, one benefit of i3DP is its capacity to satisfy various criteria in various areas. The repeatability of the surface modification of i3DP-made items when the surface is damaged is another benefit. It was also noted that this i3DP technique may be used to any ink-based 3D printing, which has enormous promise in the fields of electronics, microfluidics, antifouling, and antibacterial materials.

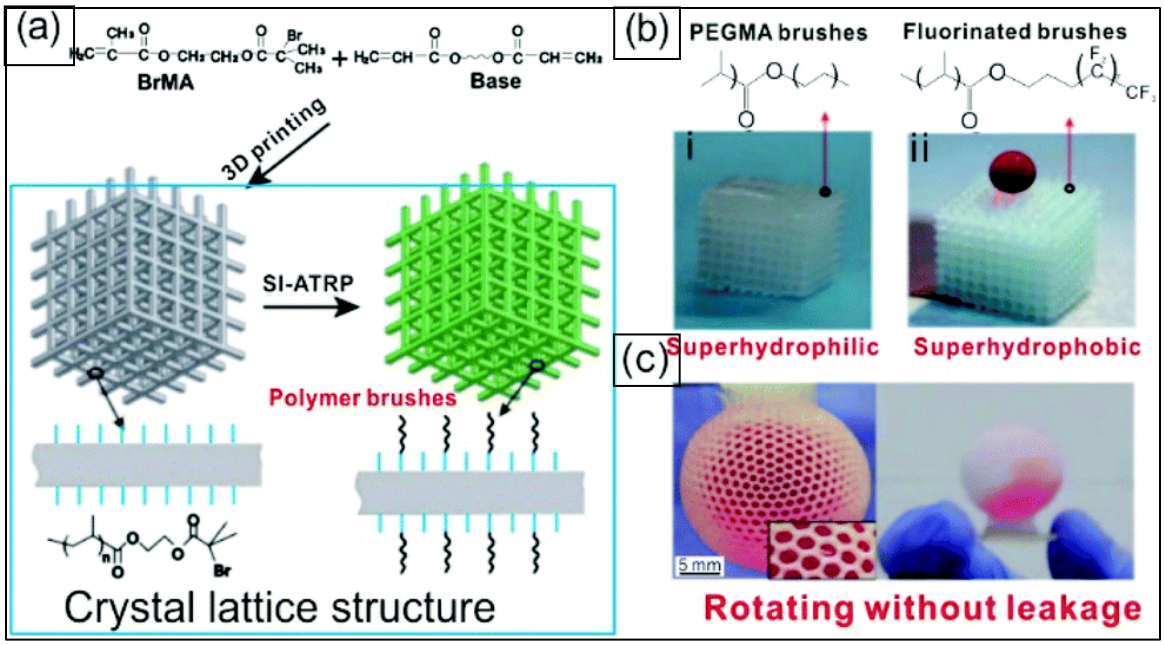

Figure 5: 3D objects with super wettability fabricated by initiator-integrated 3D printing (i3DP). (a) Schematic process of i3DP. (b) Superhydrophobic surface by grafting PEGMA brushes (left) and superhydrophobic surface with fluorinated brushes (right). (c) 3D-printed superhydrophobic ball holding water without leaking [24].

2.1.2 3D printing of superhydrophobic objects with bulk nanostructures

A new materials concept and methodology for 3D printing of superhydrophobic objects with bulk nanostructure and almost unlimited geometrical freedom is presented. A team at the Department of Applied Physics Aalto University School of Science Espoo 02150 Finland led by Zheqin Dong (2021) reported in '3D Printing of Superhydrophobic Objects with Bulk Nanostructure [46], that using a desktop Digital Light Processing (Figure 6a) printer, Superhydrophobic 3D objects with complex shapes are demonstrated, with ultralow and uniform water adhesion measured with scanning droplet adhesion microscopy. The rapid development of 3D printing technologies demands new materials with novel properties and functionalities. New materials concept and methodology for 3D printing of superhydrophobic macroscopic objects with bulk nanostructure (Figure 6e)

and almost unlimited geometrical freedom is presented. The method is based on a specific ink composed of hydrophobic acrylate monomers and pyrogen solvents, which undergoes phase separation upon photopolymerization (Figure 6b).

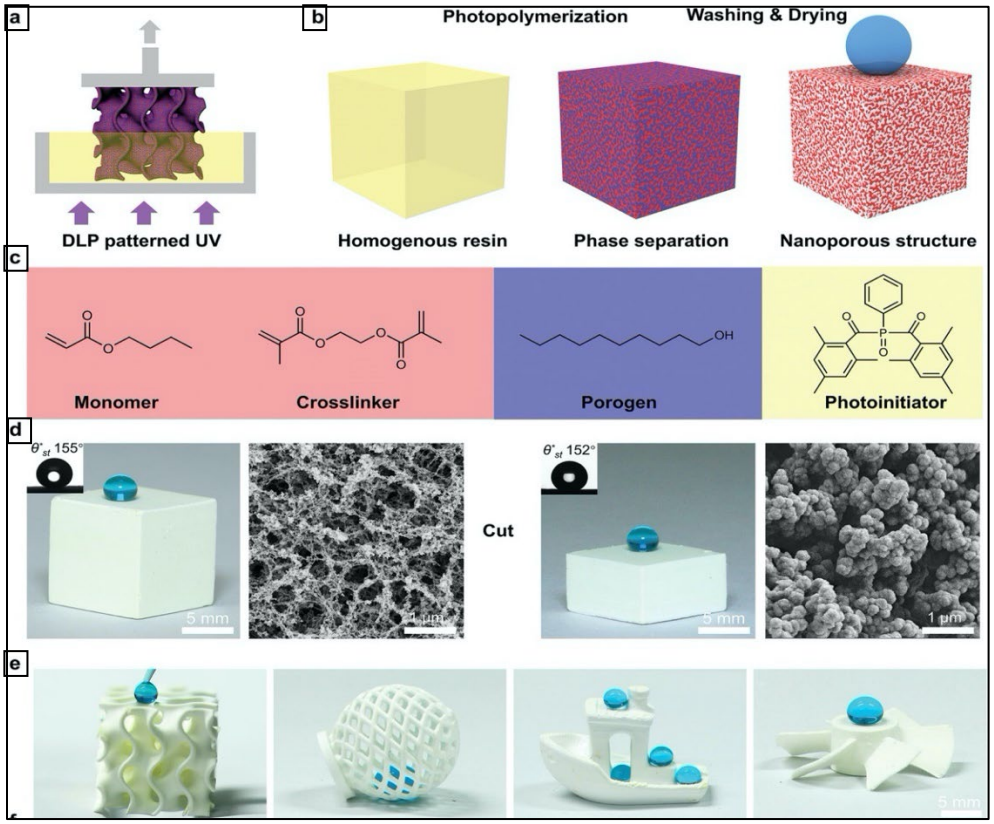

Figure 6: 3D printing of superhydrophobic objects with bulk nanostructure. a) Schematic showing the DLP 3D-printing process using a phase-separating ink; b)In this process, photopolymerization induces phase separation of the homogenous ink and generates the inherent nano porous structures leading to bulk superhydrophobicity. c)Chemical structures of the components of an exemplary ink: BA as the monomer (30 wt%), EDMA as the crosslinker (20 wt%), 1-decanol as the porogen (50 wt%), and Irgacure 819 as the photo initiator (2 wt% relative to reactive monomers). d) Photographs of dyed water droplets on the surface (left panel) and cross-section (right) of a cube printed using the phase separating ink, with the insert showing the measured static water contact angle (ϑ^*_{st}). The nano porous structure of the cube is shown in the corresponding scanning electron microscopy (SEM) images. e) Complex-shaped superhydrophobic objects printed using the novel ink demonstrating the design flexibility.
Copyright is from [46]

The nano porous structure of the cube is shown in the corresponding scanning electron microscopy. Complex-shaped superhydrophobic objects printed using the novel

ink demonstrate the design flexibility. The rapid development of 3D printing technologies demands new materials with novel properties and functionalities. Using a desktop Digital Light Processing printer, superhydrophobic 3D objects with complex shapes are demonstrated, with ultralow and uniform water adhesion measured with scanning droplet adhesion microscopy

2.1.3 3D printing of mechanically durable, super-repellent microcell/nanoparticle surfaces

Researchers have developed 3D printed re-entrant micropillars that retain their super-repellency after 100 cycles of mechanical abrasion. In 'Mechanically durable, super-repellent 3D printed microcell/nanoparticle surfaces', Sajad Haghanifar and colleagues (2022) reported that three-dimensional printed re-entrant micropillars [47] (Figure7a,b) have demonstrated high static contact angles for an unprecedented variety of liquids. But they have yet to achieve this with low contact angle hysteresis and excellent abrasion resistance. They also address contact angle hysteresis and mechanical durability issues by creation of 3D printed microcell/nanoparticle arrays (Figure 7c). The structures retain their super-repellency after 100 cycles of mechanical abrasion with a Scotch-Brite abrasive pad under a pressure of 1.2 kPa. They reported on the demonstration of 3D printed microcell/nanoparticle structures that exhibit high static contact angle, low contact angle hysteresis, and high mechanical durability. The use of interconnected microcell structures as opposed to micropillars addresses mechanical durability issues. The results demonstrate new 3D printed structures with mechanical durability and super-repellency using microcell structures integrated with fluorinated nanoparticles.

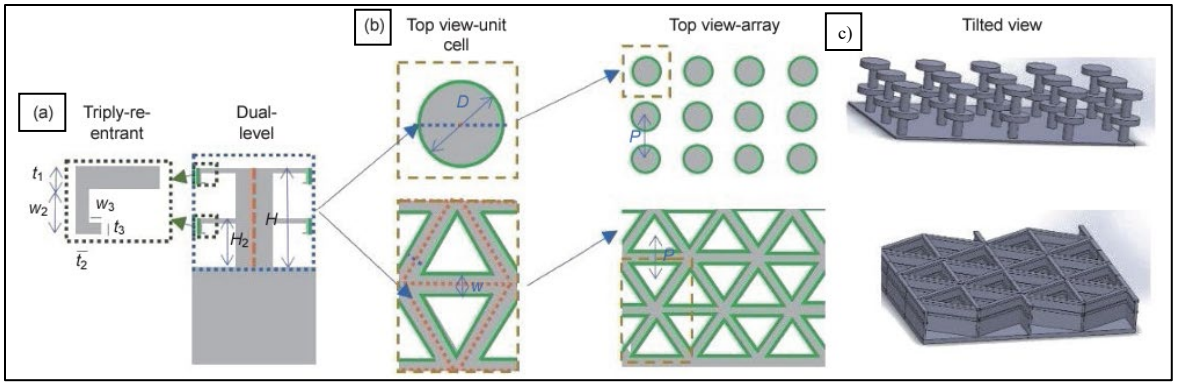

Figure 7: Schematic of dual -level triply re-entrant a) cross section for b) micropillar array and c) microcell array. The micropillar array consists of rotating the cross-section around a center axis while the microcell array consists of translating the cross-section into a triangular lattice [47].

2.2 3D Printing of Bioinspired Superhydrophobic Structures

2.2.1 Recent progress in 3D printing of bioinspired structures

Biomimicry is an area of research in which scientists look to nature for inspiration in the development of materials and structures that can be fabricated using 3DP. In 'Recent Progress in 3D Printing of Bioinspired Structures [48] (Figure 8a, b), Danfeng Wang and colleagues reported that high-performance materials and structures are currently being rapidly developed. Combining biomimicry with 3D printing technology, materials, and structures with reinforced physical properties have been fabricated for various engineering applications, some of which have been explored in this paper. Traditional manufacturing technologies cannot be used to fabricate these complex structures. Over millions of years of evolution, nature has evolved structures with relatively optimal properties. These provide researchers with valuable and useful inspiration along with tried-and tested methods for developing high-performance materials and structures. Although traditional manufacturing technologies cannot be used

to fabricate these complex structures, 3D printing can fabricate structures with arbitrary geometry (Figure8c).

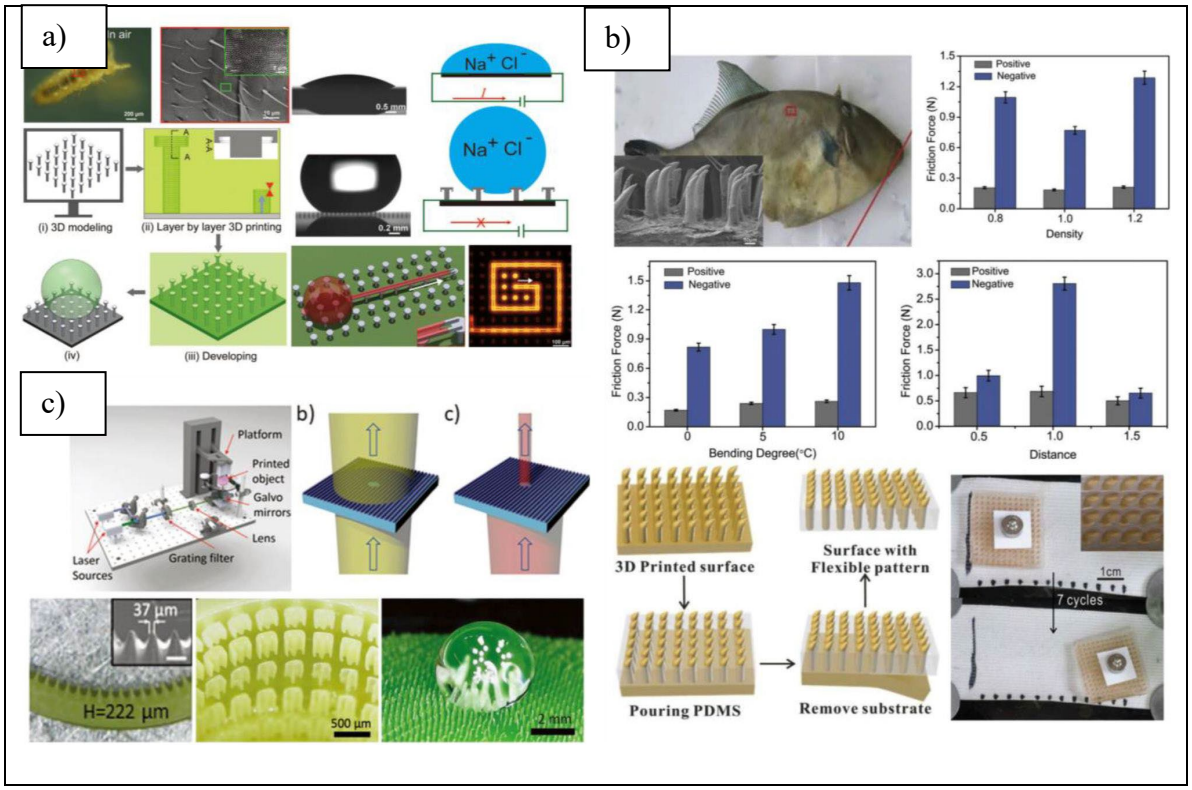

Figure 8**:** a) Triply re-entrant structures inspired by Folsomia candida, fabricated via two-photon polymerization-based 3D printing technology b) 3D printed friction anisotropic surfaces, inspired by the surface structures of the Filefish skin c) Low-cost multiscale stereolithography technology, used to print a macroscale object with microscale surface structures, inspired by shark skins and lotus leaf [48].

2.2.2 Direct laser lithography of salvinia molesta inspired micropatterned surface

A research group led by Omar Tricinci of the Center for Materials and Microsystems (2015) reported in '3D Micropatterned Surface Inspired by *Salvinia Molesta* via Direct Laser Lithography [25]' that biomimetic smart surfaces for several practical applications can be derived from the study of biological surfaces. To obtain artificial surfaces with interesting structure-related functions, they replicated the complex

structure of Salvinia Molesta hairs by downscaling it to the microscale [49] (Figure 9a,b). The structure, made with a hydrophilic material, shows remarkable functional properties, such as air trapping, hydrophobicity, and promotion of localized water condensation. Even a hydrophilic material can macroscopically behave as hydrophobic if its surface has proper micro-nanostructured features. The researchers propose a salvinia-inspired surface composed by microfabricated artificial hairs combined with a proper arrangement in arrays (Figure9c, d).

Even if the artificial hairs used in the previous tests showed the capability to support the nucleation of water droplets from the atmosphere, the best results have been obtained by changing the design of the hairs. The hairs were able to promote water condensation from environmental moisture. The micropatterned surface, in analogy with the natural model, shows interesting properties in terms of hydrophobicity and air retention when submerged by hydrophilic material. Even a hydrophilic material can macroscopically behave as hydrophobic if its surface has proper micro-nanostructured features. They investigated how the morphology can affect the functional properties of the surface as first step to develop surfaces with tailorable features. Considering the artificial salvinia-inspired structures, from a purely thermodynamic point of CB-CB and Wenzel and micro-Cassie−Baxter (W-CB) wetting regime occurs, whereas the air is always trapped inside the heads.

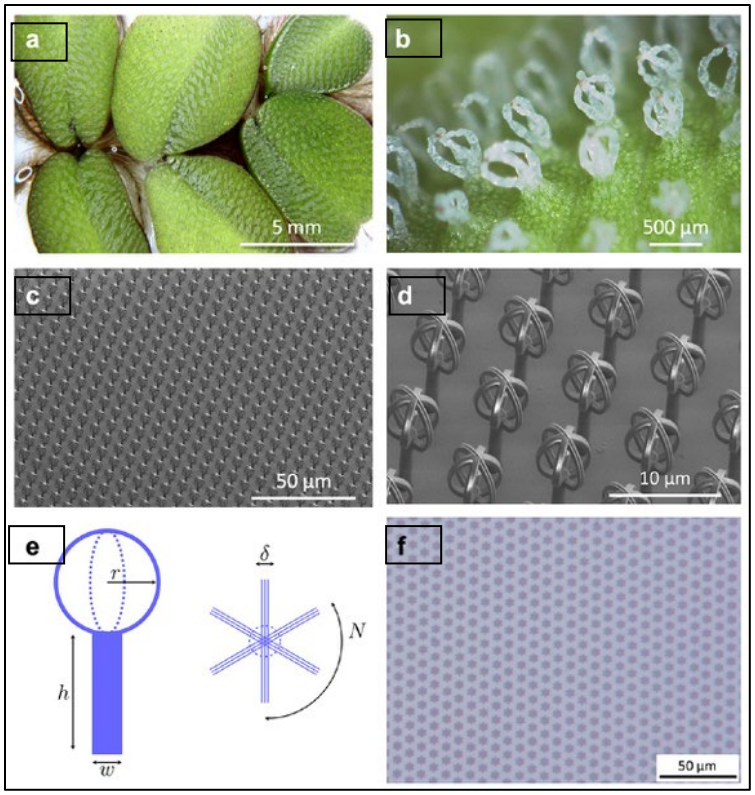

Figure 9: (a) Upper surface of Salvinia Molesta leaf covered with hydrophobic hairs. (b) Detail of Salvinia Molesta crownlike hairs. (c) Artificial crownlike hairs made in IP-DiLL photoresist on glass by means of 3D direct laser lithography. (d) Detail of artificial crownlike hairs on glass. (e) Scheme of artificial micro hairs design with geometrical parameters (h and w are height and diameter of the stalk, whereas N and δ are the number of the filaments of the head and their thickness respectively). (f) Hexagonal arrangement of the array of artificial micro hairs [49].

The growth dynamics of water droplets from vapor has been widely investigated to find a general model for this geometry-dependent property on different substrates. To assess the capability of our salvinia-inspired pattern in promoting the condensation of the water in the atmosphere, we carried out tests in a scanning electron microscope. In this paper, they extended the use of 3D laser lithography based on two-photon polymerization of a negative photoresist to the fabrication of biomimetic surfaces. In addition to the technological applications of patterned surfaces with submicrometric resolution, this

work demonstrates for the first time the use of 3D laser lithography as a powerful tool for the investigation of wettability, air retention, and condensation phenomena, opening the way to more complex studies on how microscale morphology can affect.

2.2.3 Capillary-force-induced Clustering of salvinia-inspired surfaces for hydrodynamic drag reduction

Scientists have fabricated an artificial plant leaf inspired by Salvinia Molesta, a free-floating aquatic fern, using three-dimensional printing. Many studies in bioinspired engineering have been reported to explore unique functional systems that exist in nature and use them for humans [50]. A hierarchical micro-pillar array was designed, replicated by soft lithography, and uniformly clustered by inducing capillary force. Due to its gently curved structure and local hydrophilicity, the Salvinia-inspired surface exhibited high meniscus pulling force. Because the superhydrophobic surface which has a low affinity with water loses the air lubricating layer even with small fluctuations, practical application has not been realized yet. PDMS was chosen as the replicating material to prepare the micropillar array template due to its well-established properties, including low modulus.

The Polyvinyl alcohol (PVA) solution was prepared with a low concentration for high surface tension, which could induce efficient tip clustering. Given that the hierarchical micropillar template for the capillary-force-induced clustering (CFIC) could be prepared by conventional soft lithography processes, which is easy to apply to a continuous fabrication process, it is expected to contribute to the commercialization of hydrodynamic drag reduction (HDR) surface. The mold went through a passivation process to ensure defect-less release in the following soft lithography processes.

Structural deflection of the micropillar against capillary interaction force should be considered to ensure regular clustering of the pillar arrays. Fabrication of the Salvinia-inspired surfaces by capillary-force-induced clustering. Given the meniscus pulling force and number of clustered hairs per unit area, the maximum outward pressure oscillation of the water-air interface the fabricated sample could hold without breaking a pin could be assumed as ~217 Pa. In general, an effective slip length of the surface is used to quantitatively compare the effect of HDR18. Due to its gently curved structure and local hydrophilicity, the Salvinia-inspired surface exhibited high meniscus pulling force to maintain a stable air-water interface while minimizing the water–solid contact area.

2.2.4 Salvinia inspired underwater hierarchical structures for super repellency

Biomimetic superhydrophobic surfaces display many underwater functionalities, which attribute to the slippery air mattress trapped in the microstructures on the surface. Salvinia can efficiently and robustly reactivate the invalid slippery air mattress on underwater surfaces [51]. The efficiency of the air-mattress recovery is reflected by the spontaneous transport of air in wedge-shaped grooves governed by the gas wicking effect. The finding here reveals the underlying mechanisms of the water-repellent property of Salvinia. Biomimetic superhydrophobic surfaces display many excellent underwater functionalities, which attribute to the slippery air mattress trapped in the structures on the surface. A biomimetic artificial surface that is fabricated using 3D printing technology successfully imitates the super repellent capability of Salvinia leaves to completely recover a continuous air mattress (Figure 10).

We present the underwater super repellent capacity of Salvinia, which can efficiently and robustly reactivate the invalid slippery air mattress on underwater surfaces

by trapping the replenished air to replace the water in the surface structures. The efficiency of the air-mattress recovery is reflected by the spontaneous transport of air in the wedge-shaped grooves governed by the gas wicking effect, which ensures a rapid formation of a thin air film covering the whole leaf surface. The air-mattress recovery on Salvinia leaves can be achieved on a large area and remain valid in extreme environments, such as high pressure, fluctuating waves, and even fast flows.

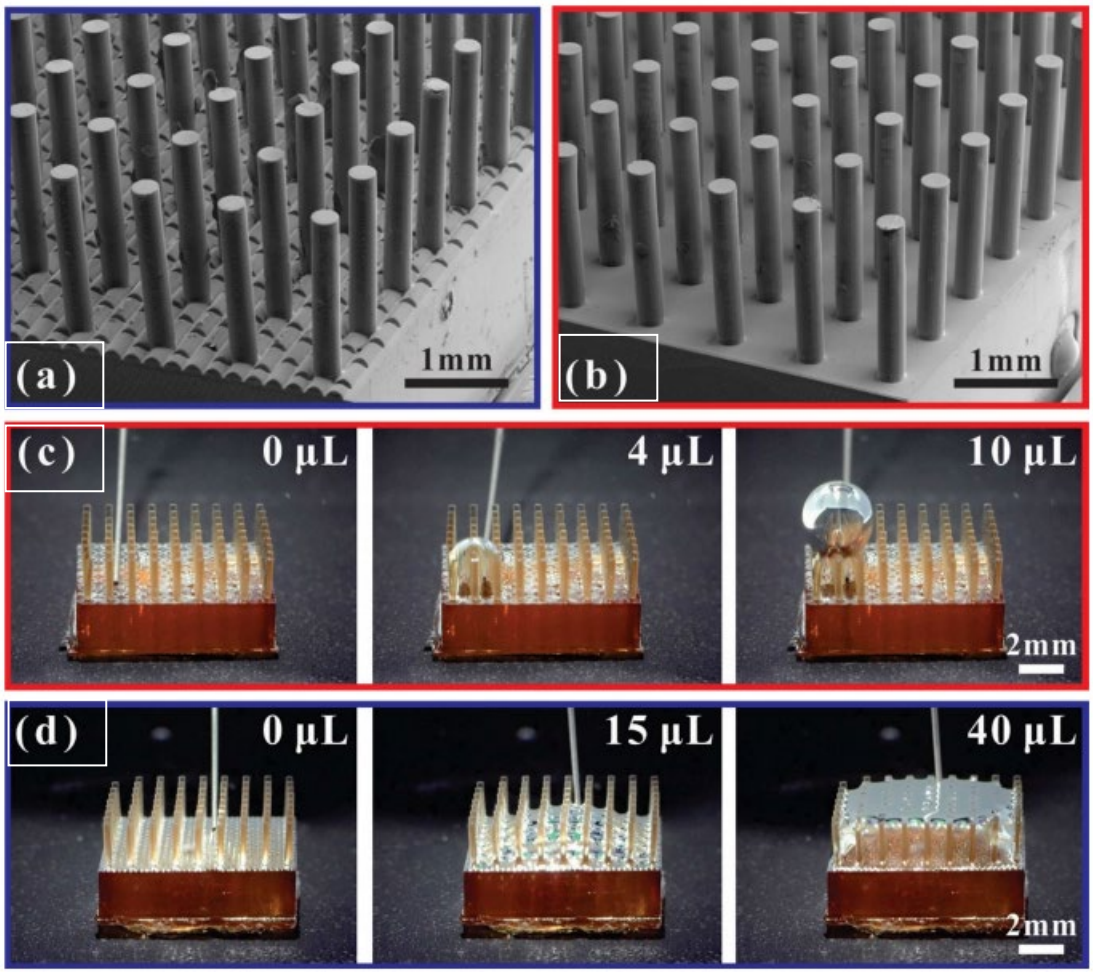

Figure 10. Air-mattress recovery process on the artificial Salvinia surface and the control specimen with post array structures. (a) SEM image of the artificial Salvinia surface. The half-cylindriform bulges on the base of the surface mimic the convex epidermal cells. The wedge-shaped grooves are formed between the bulges with the corner angle $2\alpha = 20°$. The diameter of

the post is 300 μm, the height of the post is 2000 μm, and the pitch between neighboring posts is 900 μm. The posts mimic the hairy structures. (b) SEM image of the control specimen, which has the same hairy structures (posts) as the artificial Salvinia surface in (a). (c) Air is replenished to the control specimen, where an individual bubble instead of an air mattress forms. (d) Air is replenished to the artificial Salvinia surface, where an air mattress can be completely recovered [51].

2.2.5 Immersed Surface Accumulation of Salvinia inspired eggbeater structures

A 3D-printed "eggbeater" inspired by the Salvinia Molesta leaf has been developed by researchers. Biomimetic functional surfaces are attracting increasing attention for various technological applications, especially the superhydrophobic surfaces inspired by plant leaves. The artificial surfaces with interesting structure-related functions were replicated according to the eggbeater structure design in Salvinia Molesta hairs by using a novel additive manufacturing process [52] (Figure 11a-e). The results show the 3D-printed eggbeater surface has a strong hydrophobicity and a good controllability of water droplet by turning upside down (Petal effect) as well as super-oleophilic property. Eggbeater structure with two arms is fragile and easy to break during the test. This is attributed to the increase of contact area between the eggbeater tip and the water droplet (Figure 11f, g).Some of the findings potentially confirm what was previously known about this subject: “3D cultured tumor spheroid is more resistant to drugs compared with 2D cell cultures. Cells attach to one another and form natural cell-to-cell attachments in 3D cell culture, which is flexible and pliable like natural tissues,” Yang said. Another example is the unique combination of hydrophilic path on super-hydrophobic surfaces (“Salvinia effect”), which demonstrates an effective design for long-term air retention and droplet manipulation.

In conclusion, they have demonstrated the fabrication of complex bioinspired eggbeater patterns by the ISA-3D printing process to replicate the morphology of the S. Molesta leaves. The artificial eggbeater structure, made with a hydrophilic material, shows remarkable super-hydrophobic property and petal effect. The super-hydrophobic property and tunable adhesion is related to the number of eggbeater arms and the gap distance between each hair. It opens intriguing perspectives for designing artificial surfaces on the basis of eggbeater structure to form a super-hydrophobic surface. Based on the study, they demonstrated the potential applications in the droplet-based microreactors, no loss water transport, 3D cells culture and oil/water separation via our 3D-printed eggbeater structures. They believe that the reported results would be helpful to further understand the effect of wetting states on the surface adhesion and the fabrication principle for a super-hydrophobic surface with controllable adhesion. Furthermore, considering the efficient fabrication strategy of our method, the 3D-printed structures are potentially useful in biomedical and environmental engineering, such as microdroplet manipulation, droplet-based bio detection, drug test, and massive oil/water separation.

In this study, the designed surface-based accumulation process is using the point-based and line-based CNC accumulation processes as models. In other words, a laser beam with a high-resolution 2D mask picture is used to cure materials rather than a single point spot or line beam. DMD chip technology is used to create high-resolution 2D patterned light beams, allowing the surface-based CNC accumulation method to precisely accumulate micro-scale features on the surface of an existing item. A light guide tool is created that combines an objective lens and optical fibers, allowing the light beam to

travel up to 2.5 µm per pixel, to enable constructing around inserts. When the light guide tool moves, various 2D patterned light beams may be projected while it is submerged within the resin photocurable materials. The manufacturing speed of the adding features is significantly quicker than the point-based CNC accumulation technique, and their surface quality may achieve smooth surface quality with a resolution of 5 µm. Also created numerous light guide tools to impart varied textures to various geometries, much like the CNC milling process.

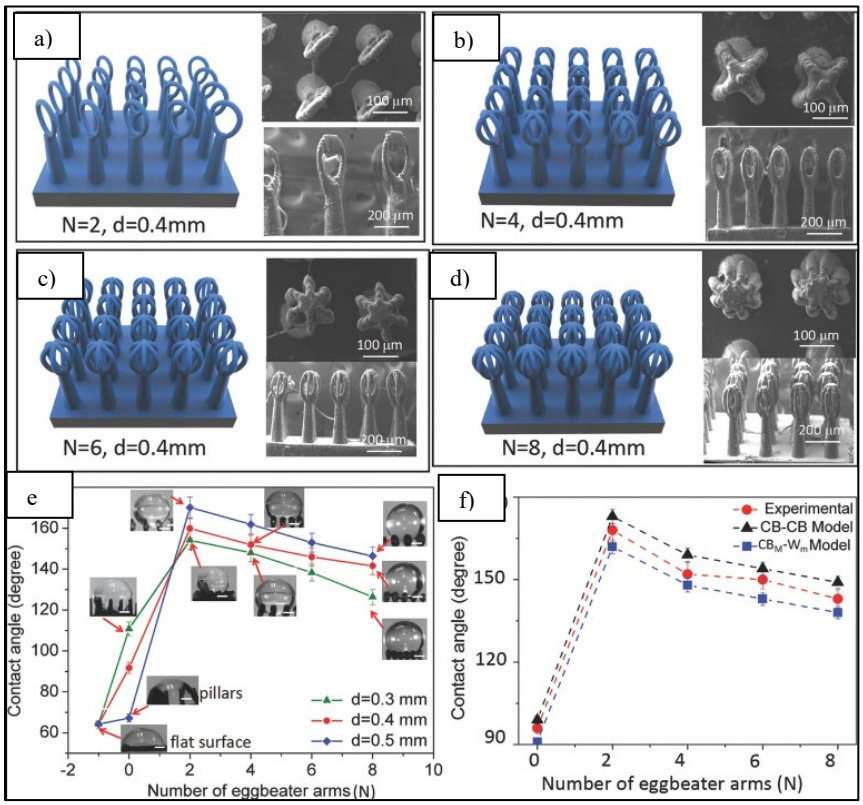

Figure 11: a) Schematic diagram of the immersed surface accumulation based 3D printing (ISA-3D) process; b) the optical system in the ISA-3D printing process (insert shows the magnification of light guide tool and optical fiber in (d) with projected 2D micro patterns); c) models and SEM image of the 3D-printed eggbeater arrays; and e) an illustration of adding microscale eggbeater structure on the free form curve surface of a lotus flower model, which changes the surface from hydrophilic to super-hydrophobic by using a straight light guide tool [52].

To demonstrate the capabilities of the new microscale additive manufacturing technology, two biomimetic microstructures have been constructed on flat surfaces. The surface performances of the pre-existing model were adjusted, and intriguing qualities were also introduced by the addition of such micro-features. The immersed surface accumulation method significantly outperforms the currently available texture fabrication techniques. The created accumulation system is also applicable to a variety of applications that call for production on several scales and materials.

A non-layer-based additive manufacturing technique is CNC accumulation [53]. Similar to the point-based CNC accumulation, the surface-based CNC accumulation employs an accumulation light guide tool to cure whatever liquid resin it comes into contact with. A movement control system, a light guide tool changing system, and an optical imaging system are all components of the correspondingly created surface-based CNC accumulation process (Figure 12). Different accumulation tools are exchanged depending on the necessary 3D textures to be created, such as the inner or exterior surfaces of an existing object, using a light guiding tool altering mechanism. To create various aspects on an item, several light guiding instruments of kaleidoscopic forms and sizes are submerged in liquid resin.

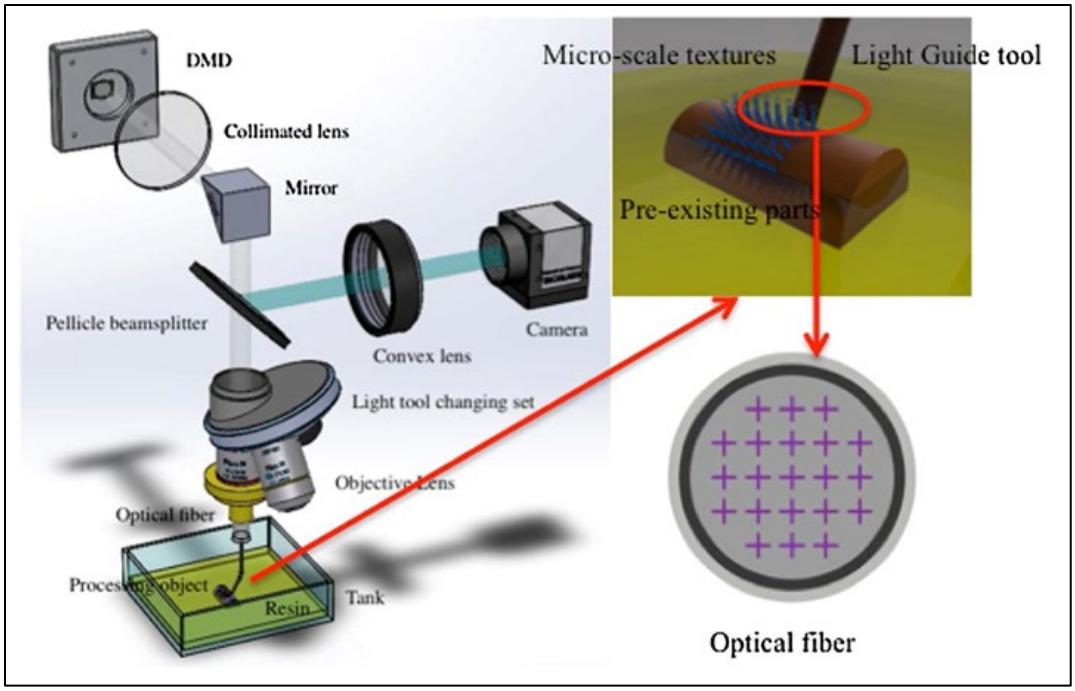

Figure 12: The layout of the immersed surface accumulation imaging system [53].

Complex eggbeater-shaped hairs coated with microscopic wax crystals and hydrophilic patches on the terminal cells dominate the hierarchical architecture of the leaf surface. Numerous attempts have been made to develop biomimetic artificial superhydrophobic surfaces. For instance, the super-hydrophobic films fabricated by electro-deposition and hydrothermal techniques with mesh like, ball cactus-like, and tilted nanorod architectures [19–21]. However, some of nature's complex designs surpass the capacity of conventional manufacturing processes, which impedes the advancement of biomimetic surface research. Lithography was used to build eggbeater structures that were one hundred times smaller than their actual counterparts in nature. However, the contact angle is only 110°-120° (not superhydrophobic) and the air volume generated on the bottom surface is limited owing to the size of these microfeatures [19]. By coating the surface of stainless steel with carbon nanotubes, high water contact angles with salvinia

effect were produced [22] To imitate the salvinia effect, additive manufacturing (3D printing) that has widespread uses in business, academia, and everyday life might be an efficient method for fabricating such complex structures [23,24].

2.3 Challenges

Three-dimensional (3D) printed re-entrant micropillars have demonstrated high static contact angles for an unprecedented variety of liquids but have yet to achieve this with low contact angle hysteresis and excellent abrasion resistance [46].

Although some high-performance bioinspired materials and structures have been successfully fabricated by 3D printing, there are still many unaddressed challenges and limits to the applications of biomimicry. For example, the tradeoff between high resolution, low cost, and high speed [47]. This is since increasing the resolution of bioinspired structures also increases cost whilst decreasing the manufacturing speed. The fabrication of multiscale structures from the nanoscale to macroscale is a challenge as to the best of our best knowledge [48], no methods for this type of fabrication currently exist. Additionally, bioinspired structures with multilateral or composite materials have typical properties and functions, and it is difficult to anticipate the effects of using different interface materials. The process of clarifying the synthesis mechanisms of different materials is another challenge in fabricating high-performance bioinspired materials and structures [49].

Considering these challenges, it is anticipated that future developments in bioinspired 3D printing will focus on multilateral, multiscale, multifunctional, high-efficiency, and low-cost fabrication [49]. For multilateral fabrication, the synthesis mechanism of different materials will be investigated and clarified to guide 3D printing.

In terms of multiscale fabrication, novel 3D printing technology will be proposed to realize continuous fabrication from nanoscale to macroscale. Bioinspired materials and structures with multifunctional properties, including reinforced mechanical, electrical, electromagnetic, optical, chemical properties, will be the research hotspots. In addition, developing high-efficiency and low-cost fabrication technologies will be an effective way to accelerate the development and application of biomimetic 3D printing technology.

Numerous innovative additive manufacturing (AM) techniques have been developed and successfully brought to market during the last few decades [43-46]. Computer-aided design (CAD) models may be produced using AM methods, which typically provide flexibility and high control over the resultant shape [43]. Recent breakthroughs in material, methodology, and machinery support the use of AM techniques to create air-tight structures with bioinspired superhydrophobic properties [20,30]. For instance, direct laser lithography was used to replicate microscale Salvinia-inspired structures, of which the dimension was 100 times smaller [20]. However, due to their small size, printed structures were unable to retain as much air, and pressure changes made it simple for the air film to quickly evaporate from their surface [47]. As shown in Fig. 1a, the exceptional micron-submicron roughness of hierarchical structures is responsible for the remarkable super hydrophobicity of Salvinia Molesta leaves [14-26]. *Current 3D printed bioinspired surfaces, in contrast, have difficulty replicating such dual-scale roughness, which prevents printed materials from performing as well in terms of liquid repellency and air trapping as natural structures* [48-52]. The simple solution to this issue is to apply a thin layer of low surface energy coating to the printed structures to

improve their nanoscale roughness [42,53,54], however this extra coating of nanolayer would deteriorate over time due to abrasion and lose its adherence [48].

2.4 Principle and Methodology

In some of the previous studies, these Salvinia based biomimetic structures have been made using different photopolymer resins. But using just the resin is hard to increase the surface roughness properties at multiscale while printing. But it is much easier to print and adjust the printing parameters while using these pure resins. The size, number of eggbeater arms, and gap distance were all variable so that it would be possible to examine how they affected the hydrophobic property and water adhesion. Here to achieve the multiscale roughness, at microscale the printing level is easy to achieve but nanoscale wax crystal like roughness is hard to achieve without any fillers. *The hypothesis is that the Multiwalled carbon nanotubes (MWCNTs) were additionally included in the liquid resin to both improve surface roughness at micro-scale and eliminate static charges generated on surfaces with its high conductive nature.* Also, the electrical properties help in their alignment when introduced under electric field. Both the chemical composition and the geometric structure of an eggbeater surface influence its unique wetting properties.

Using multiwalled carbon nanotubes to create superhydrophobic structures, electrical assistance is used in additive manufacturing and 3D printing (MWCNT). A stable and continuous voltage source is used to regulate the alignment of MWCNT, and it is investigated how to employ this control to provide superior mechanical characteristics. Due to their distinctive structural characteristics and excellent mechanical qualities, carbon nanotubes (CNTs) have shown significant promise as multifunctional nanofillers

for polymer-based nanocomposites. To further enhance the multifunctional characteristics, controlled alignment of CNTs in polymer matrix by electric field will be studied. This helps us get better roughness properties at nanoscale. *Thus, the superhydrophobic structures with multi-scale roughness at micro-scale due to the dispersion of MWCNT and at nano-scale due to the alignment of MWCNT can be achieved.* In the above, we describe a method for fabricating biomimetic superhydrophobic eggbeater structures with tunable surface shape. Using a unique additive manufacturing technology called Vat Photopolymerization [2] 3D Printing (VPP 3DP) (figure 13c), artificial surfaces with intriguing structure-related functionalities were recreated in the hairs of Salvinia Molesta in accordance with the eggbeater structural design.

A novel 3D printing method called Electrically Assisted Vat Photopolymerization (e-VPP) based on Vat Photopolymerization (Figure 13b) has been developed. The essential element of the VPP-3D printing technology is a light source like a projector and a guide tool to act as a build platform. The guide instrument is submerged in a tank containing photocurable liquid resin (MWCNTs) (Figure 13d). The vat tank is setup with two copper electrodes (Figure 13c, d) facing each other that are connected to AC high voltage source. The electric field is used to align the orientation of MWCNT present in the photopolymer resin. The e-VPP-3D printing process may create microscale details on the surface of a macroscale item by selectively curing liquid resin into solid by combining dynamically controlled light beam projection with the single-axis movement of the guide tool.

Unlike other additive manufacturing technologies, e-VPP-3D printing permits the modification of an object's surface functionality. For the process of surface accumulation, a straight light beam (light intensity of 28.5 mW/cm2) resin (Figure 13f) is projected onto the liquid photocurable, and the guide tool is immersed completely until it reaches the bottom of the tank resin (Figure 13e) leaving a gap for the photopolymer resin to cure and turn into a solid object. Consequently, the resin is hardened by the 2D patterned light beam on the surface of the guided flat surface. After the first cured layer has been adhered to the inserted item, the guiding tool retreats at a predetermined pace. Since the guiding tool is submerged in liquid resin, enough resin will fill the curing region throughout the movement. Thus, a structure is created after multiple iterations. This technology enables the production of multiscale patterns on the surface of a structure by accumulating material along the path of a light guide tool inside a photocurable resin. In addition, the controllable characteristics (size, number of eggbeater arms, and gap distance) were modified to examine their impacts on hydrophobicity and water adhesion. In addition, multiwalled carbon nanotubes (MWCNTs) were included into the liquid resin due to their capacity to eliminate static charges and improve surface roughness [25,26]. The peculiar wetting qualities of the surface of an eggbeater are regulated by both its chemical composition and its geometric structure.

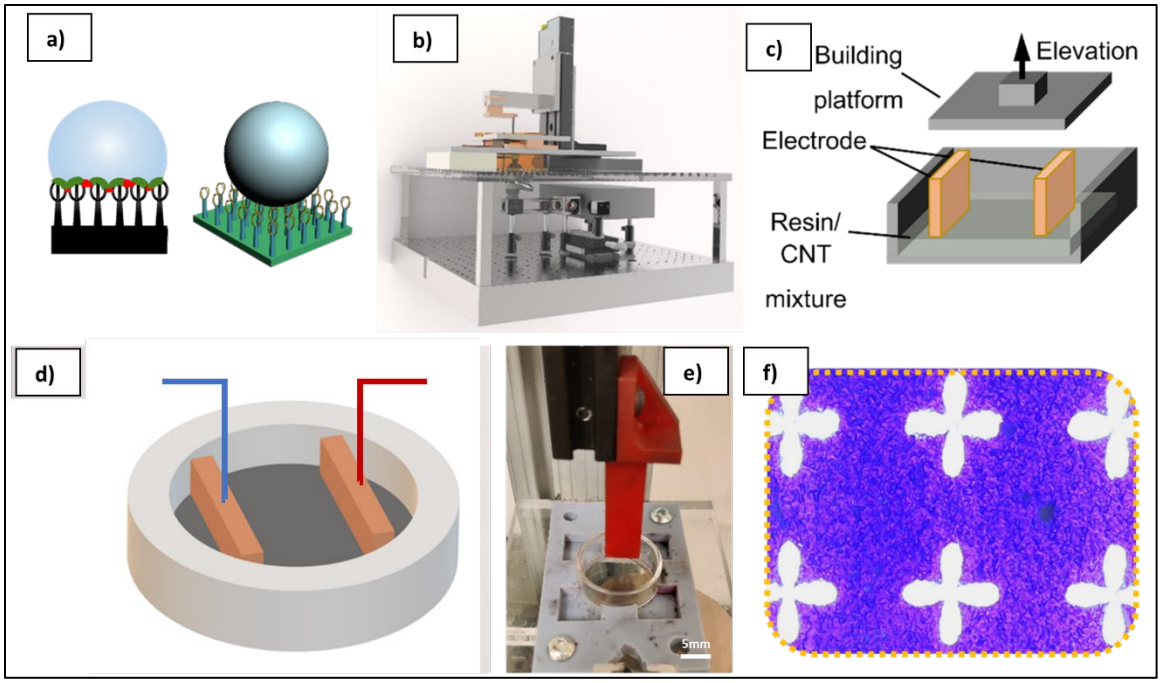

Figure 13: a) Hydrophobic and Superhydrophobic Structures [52]. B) e-VPP 3D Printing CAD [53] Model. c) Vat tank with resin and the electrode setup. d) Vat tank and flat guided tool setup. e) Light beam projected on the tank surface.

CHAPTER 3

EXPERIMENTS AND METHODOLOGY

3.1 Material preparation

In Vat Polymerization, the photocurable resin is cured when a light is projected on to it. MakerJuice resin is a UV curable commercial photo polymer resin with a viscosity of 220cp. It also has a Modulus of 655 MPa and tensile modulus of 47 MPa. The viscosity of photo-curing UV resin for bottom-up photo-curing techniques, where the light source is below the resin vat and the cured component is pulled up, UV resins play an important role in adhesion to the build plate. Viscous forces pull down on the component as the material at the bottom of the vat cures and the moving platform is lifted, enabling the separation of the part from the build plate. This may be compared to pulling a rod out of tar as opposed to water. As they relate to the applications and functionality of the finished printed item, the final mechanical properties of cured parts are crucial. The ability to cure resins with specific processing conditions (exposure intensity, exposure duration, layer thickness), as well as to compare a resin's final properties when subjected to changes in processing conditions, is facilitated by the complex shear moduli of the materials as the cure progresses.

This Red Resin is mixed with MWCNT at 0.5%, 1%, 1.5%, 2% and 2.5% of total weight percentage. These materials can be homogenously mixed using different techniques. Some of them are Magnetic Stirring, Ultrasonic Mixing and Vortex Mixing.

Magnetic Stirring: It is a technique where the material is mixed using a magnetic stirrer on a electro-magnetic surface which rotates at high speeds which creates rotating magnetic field and helps the material to disperse quickly (Figure 14a).

Vortex Mixing: It is a technique where an electric motor is connected to a drive shaft oriented vertically and attached to a rubber piece mounted slightly off-center. The material is placed on this rubber piece at high speeds for a good mixture (Figure 14b).

Ultrasonic Mixing: When the material is placed in between ultrasonic waves, a cycle of alternating high and low pressure eventually creates vacuum bubbles in the material to rapidly form and collapse. This creates shear and shock waves which helps mixing the material (Figure 14c).

Figure 14: a) Magnetic Stirrer. B) Vortex Spinner. C) Ultra sonic Bath.

3.2 Electrical Field Generation Module

The Experimental setup consists of a custom-made 3D printer setup using uni-directional actuator (Figure 15a), UV Light Projector (Figure 15b), A stepped motor and a controller. As Digital Light Projection 3D Printing is a layer-by-layer process, a unidirectional actuator is used for z-axis moment. The light intensity from the projector is manually fixed to control the rate of curing and to control the quality of printing. To

block the excess light emitted from the projector during the printing process, a shutter blocker is attached to the stepped motor. The actuator and stepped motor are connected to KFLOP controller which is connected to the computer. The above-mentioned parts are connected to a power source. KMotion Software is used to operate these devices. To operate the experiments at high voltages, HIPOTRONICS HD100 Series of AC/DC Hipot Tester (Figure 15c) is used. It handles output voltage control for the experiment.

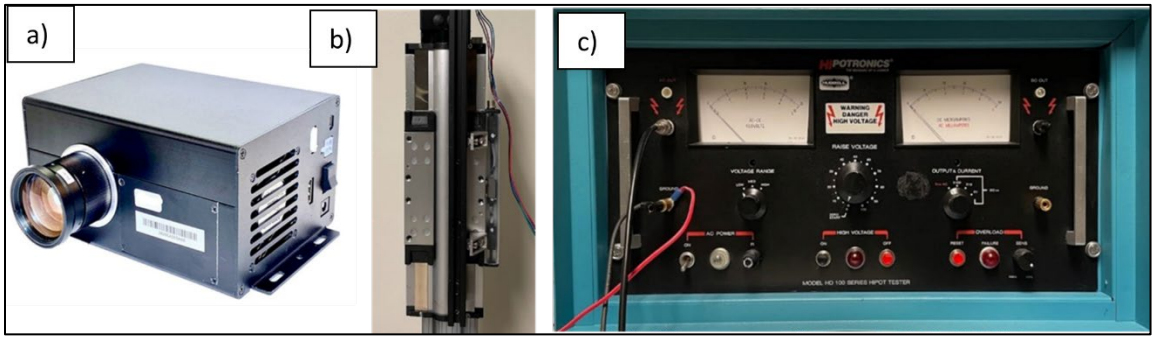

Figure 15: a) UV Projector. B) Single- axis actuator. C) Hipot Tester for Voltage Adjustment.

3.3 Electrode setup for MWCNT Alignment

Two copper electrodes are placed inside the either side of the glass tank with a distance of 20 mm (Figure 16a) and these are connected to the positive and negative AC outlet of the Hipot tester. The electricity is controlled by regulating the voltage parameters from the tester. The voltage is always set in between 1KV to 2KV as it is enough to align the MWCNT of 0.5%, 1%, 1.5%, 2% and 2.5% MWCNT weight percentages that are used to print. The voltage is controlled during the VPP process at the Hipot Tester manually to align the MWCNT present in the polymer resin while the other components of the setup like Linear Stage actuator and the projector are working on the

printing process. The connections of the setup are explained using a chart in the Figure 16b.

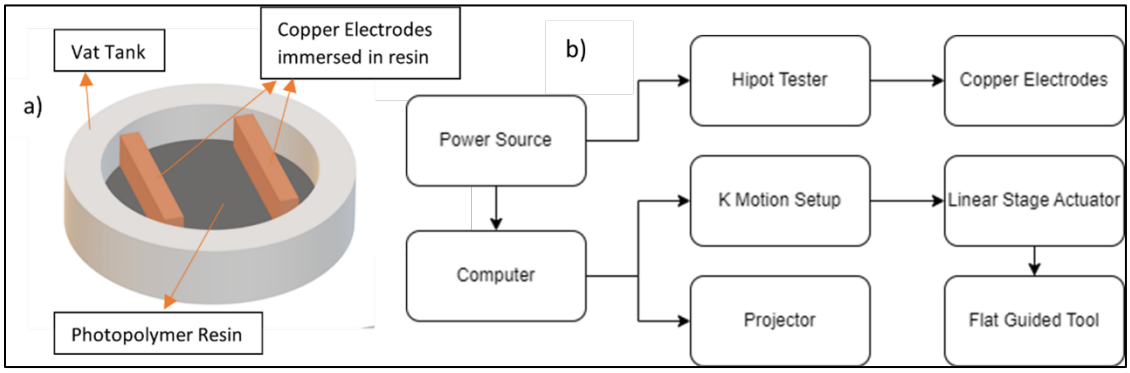

Figure 16: a) CAD Model of the Copper Electrode Setup in the Vat Tank; b) Schematic Description of different connections between the components used in the setup.

3.4 Electrically assisted vat photopolymerization

Vat Polymerization is a technique used in 3D printing. Photopolymerization process is emitting UV light onto liquid polymer resin to convert that liquid resin to solid. It is also called Digital Light Projection. In Vat Polymerization Process (Figure 17a), a transparent tank is filled with liquid resin and is positioned in a way that the UV light is emitted onto one of the surfaces of the resin. Digital Light Projection 3D Printing, a novel manufacturing method where we project the horizontally sliced images of the structure one after the other on the photocurable resin to create a photopolymerized structure. After curing one layer, the cured layer is lifted and then lowered on to the bottom surface of the tank using a guide tool which acts as a build platform with the help of the single-axis actuator. This process is continued until the structure is completely printed and finished. This process helps us create the structure with controlled micro scale surface roughness

which is hard to control using traditional methods. The light intensity of a 2D patterned light beam transmitted by the UV Projector varies according to the positions. It follows Gaussian Function. The original light intensity distribution of the whole exposure area is a patterned mask image and the light beam generated from the fabrication process of biomimetic eggbeater shaped structure before optimization are projected onto the surface of the resin. Some portions of the projected light are over-cured while other portions cannot be sufficiently cured under the same time exposure due to the non-uniform light intensity distribution because of the neighboring pixels. Such non-uniformed light intensity from the light guide tool significantly impacts the accuracy and resolution of the VPP-3D printing. To address the problem, the light intensity distribution of the 2D patterned light beam was calibrated. Here the UV Projector is adjusted in a way that the light is directly projecting onto the bottom surface of the resin tank. The UV light intensity is manually controlled and fixed at 30% to avoid over-curing of the resin which would result in irregular shapes and patterns in the finished structure. The focus of the image should also be tested before each print to ensure the quality of the print.

In between the layers, there will be a time gap, time taken by the guide tool to lift the printed portion and come back to the bottom of the tank. The UV light coming from the projector in these intervals has the ability to cure the resin to some extent. This causes irregular strands of cured resin in between the printed structures and is hard to clean. This problem is better avoided using a stepped motor operated shutter that helps block the UV light in time interval between each layer (Figure 17c).

The immersed electrode setup (Figure 17b) inside the resin is connected to a AC High Voltage output, where the voltage parameters can be altered. This way, the VPP

process is used with the help of electric field to align highly conductive materials like MWCNT which are added as nanofillers to the photopolymer resin that will be cured to print solid structures.

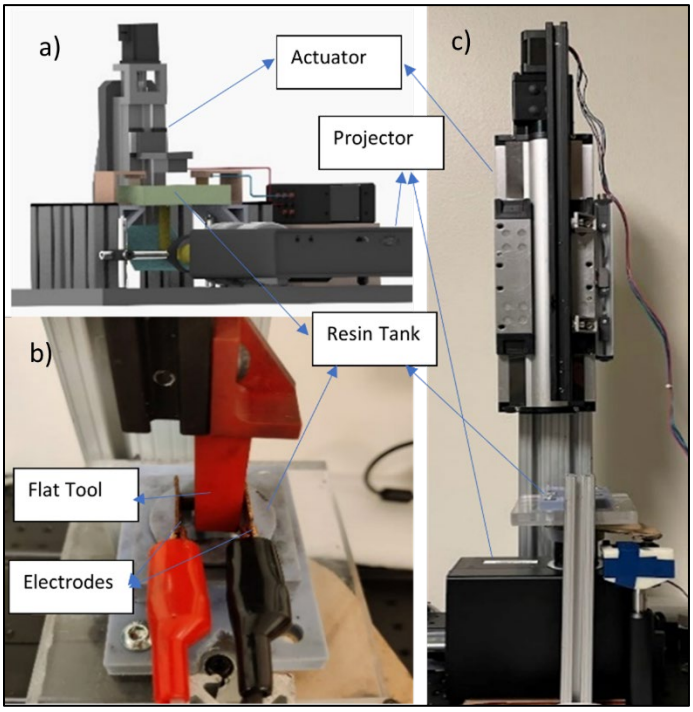

Figure 17: a) CAD Model of VPP 3DP [11]; b) Electrode Setup; c) e-VPP Setup

3.5 Slicing for Mask Projection Images Generation

The CAD model (Figure 18a) which is designed in SolidWorks, is altered in size and its position in a 3D space using Meshmixer software. The original CAD model is converted into an STL file, and the dimensions are accurately altered comparing the size ratio between the CAD model that is to be projected and the real size of printed part. Then this model is sliced horizontally for 50µm using the KMotion Slicer Software (Figure 18b). Thus, the set of sliced images (Figure 18c) which are used as masked images, are needed for the printing. The number of images obtained is completely based

on the depth of slicing of the CAD model which also represents the curing depth. The sizing of the CAD model plays an important role as it can completely change the real size of the printing structure. All these images are stored in a folder and are used to print the structure by printing them one after the other.

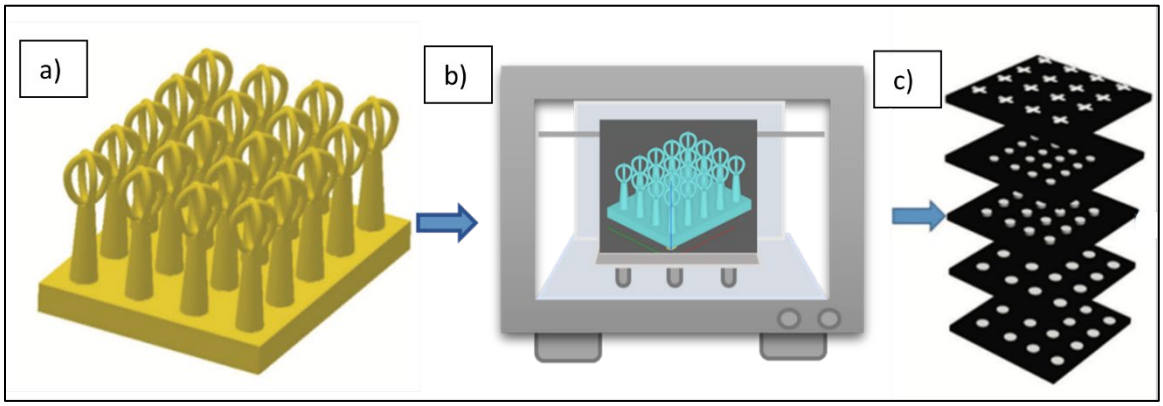

Figure 18: a) CAD Model of Eggbeater Structure [12]; b) Slicing Software Interface when the CAD Model is uploaded for slicing; c) Sliced Images which are used for projecting.

3.6 E-VPP of Eggbeater shaped Structures

The images are projected one at a time from the projector onto the bottom surface of the vat tank after being split into slices for VPP 3D printing. The program that projects these masked images onto the bottom surface of the vat tank uses a set of sliced photos that are saved in a folder. To prevent any form of movement, the vat tank is fixed in every direction. If the vat tank is not securely fixed in place, the printed structures could lose the appropriate shapes and properties. Additionally, this alters the projector's focus and the printing resolutions, which might result in distorted shapes and poor print quality. In order to allow the UV lights to cure a layer and print it on the flat tool, the flat guiding tool is adjusted such that there is some resin between its lowest point and the tank's bottom surface. The exposure time, the number of layers to print, the flat tool's travel

distance, the layer thickness, and the images to project are all controlled by the programming software. As a result, the first layer is printed on the flat tool's bottom surface after the first image is projected onto the photopolymer resin. Based on the layer thickness specified, the flat tool is then raised to create a new layer and lowered in a control motion to allow more resin in between for the following layers. Then a structure is printed following several iterations.

Images with high-intensity light are emitted by the UV projector. The photopolymer could overcure as a direct result. So, the UV Projector's intensity is decreased to 30% of the total intensity. Throughout the project, curing times for the material are tracked with a 30% intensity. A shutter connected to a stepping motor is used to block the light in order to prevent overcuring between individual layers (extra light from the projector during the breaks). It is programmed to open when the image is projected and close based on the exposure time after the projection.

The flat guided tool (Figure 19c) of 15mm* 15 mm is made of the same MakerJuice resin because of its use in the electric field and to improve adhesion between new prints and the tool surface. To improve adherence with freshly printed parts, the fat tool surface is roughened with a flat file after each print. The regulated speed, which is based on the number of layers to be printed, determines how quickly the flat tool lifts and lowers for each print. Here, the flat tool is raised 10 layers of 50 μm thickness, or 500 μm with a speed of 50 μm/sec, for each individual image projected. By doing so, the shape of the structure that will be printed can be managed, and the printed layers can be raised without being damaged. These prints' surface roughness is always influenced by printing speed and print layer depth. Similar to other 3D printing processes, the shape of the

structure improves with slower printing speeds. The mixture and its curing properties have a complete effect on the layer depth and exposure time.

All other printer setup parameters remain constant while the MWCNT present in the photopolymer resin is aligned utilizing an electric field. High Voltages are delivered to the electrodes (Figure 19a, 19b) connected to the Hipot Tester. The actuator, the flat tool, can be put to sleep for a period of time to allow MWCNT to start aligning at these voltages. When using the Hipot Tester, the setup is unaltered. If these AC High Voltages are continuously applied to the resin mixtures, the MWCNT will become very conductive and adopt the structure of a long chain. When current begins to flow through them, the Hipot Tester will shut off promptly. This will be covered in section 4.3. Hipot tester must be turned off after printing is complete before moving on to the next step.

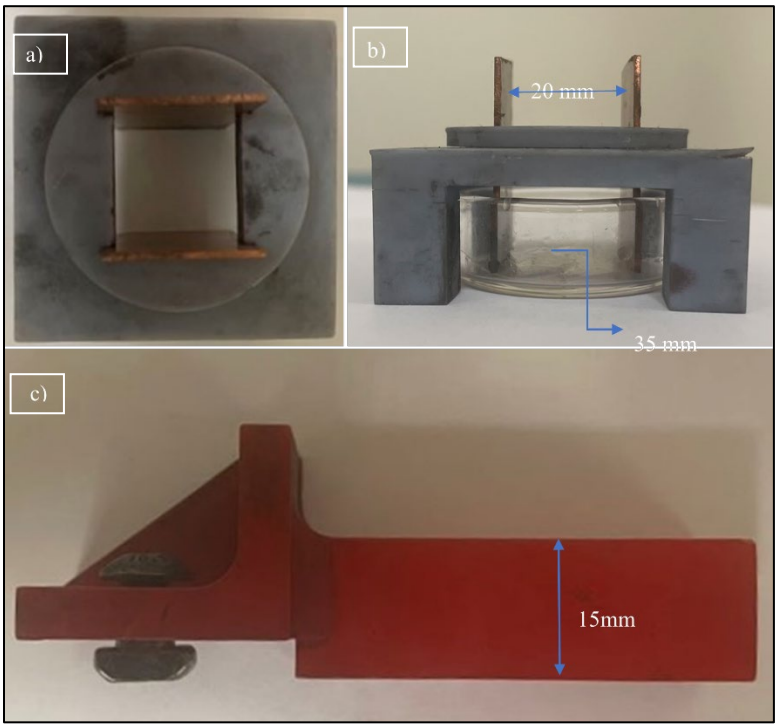

Figure 19: a) Top view of the electrode setup in vat tank; b) Side view of the electrode setup. c) Flat Guided Tool Side View.

To print these eggbeaters using e-VPP, a vat tank of 35mm diameter is filled with the MWCNT mixed resin. After the printing process, a flat base with a thickness of 400 μm is created so that the eggbeaters can stand upon it. Next, the eggbeaters' stems and then the smallest component, the eggbeater heads, which have a size of 50 μm each, are printed. Because this method of production is bottom-up, the printed parts are adhered to the flat surface in the reverse direction and must be peeled off of the tool for additional testing. The printed item has a rectangular base with a total size of 11mm*9mm, with a base of 400μm, and a total height of 1.75mm. After the printing is finished, the printed part is cleaned in ultrasonic bath for 3-5 min for the excessive resin to wash off and then it is dried. Then the printed part is used for further tests.

3.7 Mechanical Simulation

The CAD Model is designed using SolidWorks and is uploaded to COMSOL Multiphysics for the simulation of free fall of a water droplet on the heads of eggbeater structures. By using the droplet gravity, it was possible to model how water droplets would compress on a 3D-printed eggbeater structure [12]. A spherical ball of radius 750μm is created and the material properties of water droplet are given to it. The weight of this water droplet created is around 1.76mg which is around 1.76e-3mL. A relatively homogeneous material was selected for the eggbeater structures and a 1.95 GPa modulus was chosen for the structure made with Red Resin. Whereas for the 0.5% MWCNT mixture 2.13GPa and for the aligned mixture 2.29GPa are considered. For the simulation, an array of 4*1 is designed for the eggbeaters. The water droplet is assumed to be stationary, and the applied force is the gravity, 9.8m/s^2, is given to the droplets to

study the deformation of eggbeater arrays which is 17.2μN. In order to observe the deformation of eggbeater arrays in different direction, a side force was also applied at an angle of 45° which gives a load of 12.16μN on the eggbeater structures.

3.8 Wettability Evaluation

Wettability is the ability of a liquid to maintain the contact with a solid surface, and it is controlled by the balance between the intermolecular interactions of adhesive type and cohesive type [33]. Contact angles have a lot of practical applications. The average wettability of a materials system can be determined by evaluating them on a macroscopic scale. The shape of the macroscopic fluid body in different geometries may really be predicted by understanding the macroscopic contact angle for a materials system as well to whether a liquid droplet would stay up on or spread out across a solid surface. Contact angles are essential in assessing wettability in a lab setting and forecasting the wetting behavior of the same material system in geometry or technological process due to their macroscopic nature.

The contact angle can be measured by using a Contact Angle Goniometer (Figure20a). The specimen that needed to be tested is placed on the Flat Surface of this machine and is fixed on it. Then the syringe which is already fed with water using the software and then it is positioned in a way that the tip of the syringe is near the heads of eggbeater structures. A water droplet of controlled volume is dropped on these eggbeater heads to observe the superhydrophobicity property of these structures. If the water droplet stays on top of the eggbeater heads, then the Camera (Figure 20b) is used to take pictures of it and then the Contact Angle is calculated using ImageJ software. The water

is dropped at a rate of 0.5µL/sec onto the surface of the eggbeater heads. This can be manually controlled until the drop is observed floating on the structure as shown in Figure 20c.

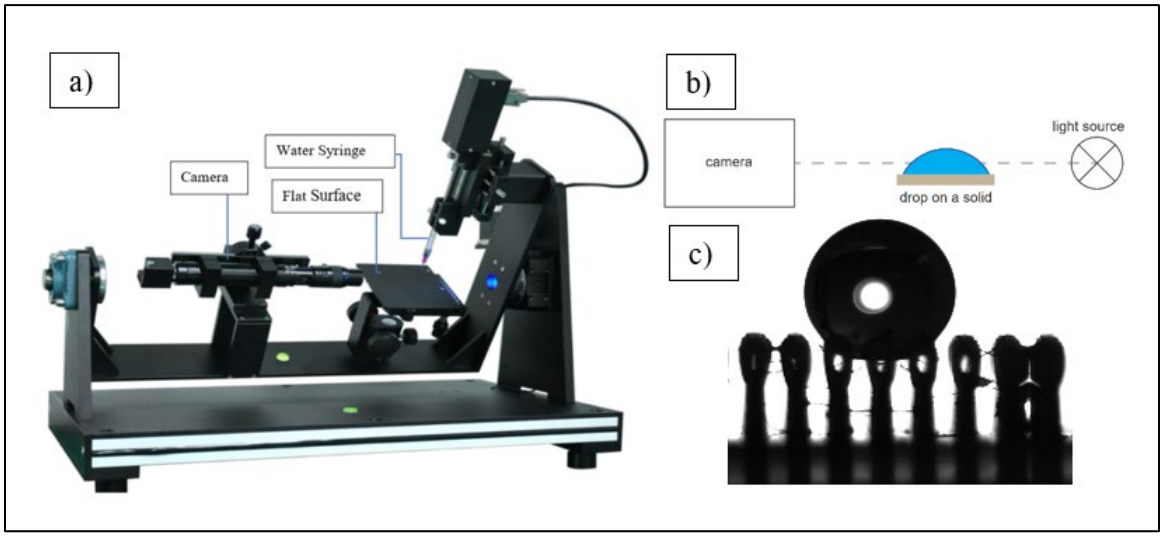

Figure 20: a) Contact Angle Goniometer; b) Image capturing for CA Measurement. c) Image showing a water droplet Floating on the eggbeater structure.

The contact angle observed for the experiments are calculated from the images taken from the Contact Angle Goniometer using a software called "ImageJ" [12] (Figure 21) which uses multiple data points as input and compares them with the standard measurements of contact angles. An ellipse is taken and is set into the shape of the water droplet that is being observed on the top of the superhydrophobic eggbeater structures. The top-most edges of these heads are considered as the base for these ellipses formed and the CA angle is measured from them.

Normal size/volume of the droplet varies from 5-7.5 µL depends upon the rate of drop which can be manually controlled to observe the Contact Angle made by the droplet. The

setup should be used in a way that no external factors should cause disturbances while capturing the images for contact angle measurement like air flow or heavy vibrations.

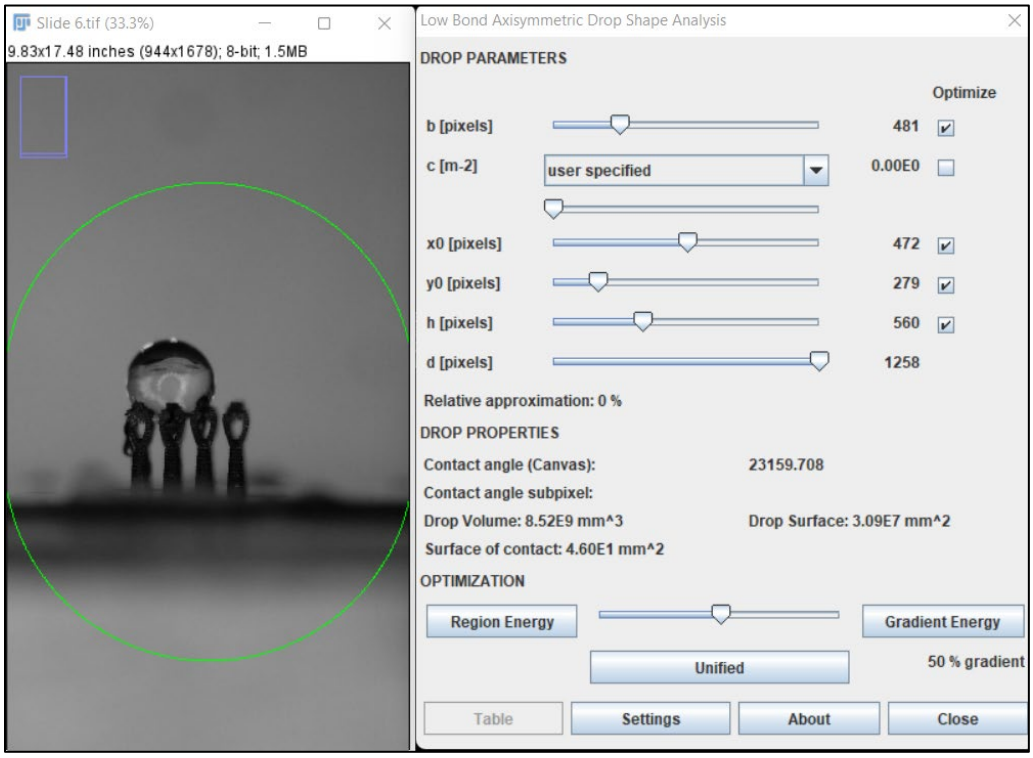

Figure 21: ImageJ Software and its interface

3.9 Attaching Force Measurement

A 3D-printed eggbeater structure is placed between a luminous screen and an optical microscope over a tank of colored water for the adhesive force test (Figure22a). The 3D-printed eggbeater structure is lowered vertically into the surface of the colored water attached to the flat tool connected to a stepper motor. When the eggbeater structure is extracted from the water's surface, a meniscus will be developed. To demonstrate the effects of pinning, individual eggbeater hairs were submerged in water [34]. From a lateral perspective, the form and size of the water meniscus generated by removing hairs from water were recorded. As a measurement of hydrophilicity, the distance between the hair's

tip and the water's surface at the precise moment the meniscus snaps off y(x) (Figure 22b) was measured.

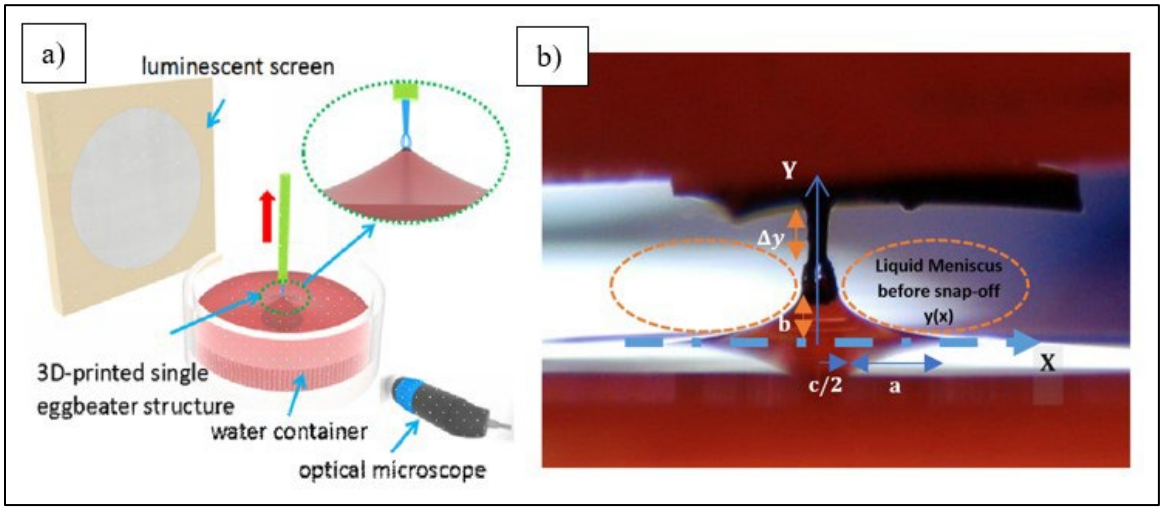

Figure 22: a) Attaching force measurement [3]. b) a,b and c examples for elliptic equation.

3.10 Surface Roughness Measurement

High contact angles (CA) with water are ideal for superhydrophobic surfaces. In order to have low CA, superhydrophobic surfaces should be able to establish a stable composite interface with air pockets between solid and liquid, while high CA may be obtained by increasing surface roughness. The capacity of a solid surface to reject water, or hydrophobicity, is a crucial quality for these eggbeater structures. It is commonly recognized that a hydrophobic material's roughness may considerably increase the contact angle (CA) it has with a liquid, which is one of the key factors determining hydrophobicity. The CA describes how much of a droplet is in touch with a solid surface. The contact area between a liquid droplet and a solid decrease with increasing CA, as does adhesion and resistance to droplet motion. The process of roughness-induced hydrophobicity is complex and has implications for a variety of scales. For It is crucial that a composite solid-liquid-air interface be produced for the majority of

superhydrophobic surfaces. An integrated interface reduces a liquid droplet's ability to stick to a solid surface by drastically reducing the area of contact between the two. The relative sizes of the liquid droplet and the specifics of the roughness rely on the production of a composite interface, which is a multiscale event. Because the change to a homogeneous interface is irreversible, the composite interface is brittle. Convex surfaces and multiscale roughness may both aid prevent instability. Surfaces that pin the contact, bringing about a steady balance and avoiding the filling of spaces between the pillars even when the substance is hydrophilic. Multiscale roughness is needed in order to withstand these scale-dependent phenomena. These superhydrophobic surfaces have such multiscale roughness. A cube of 5mm is made up of 0.5%, 1%, 1.5%, 2% and 2.5% MWCNT weight percentages with random alignment and alignment under electric field respectively using a sliced CAD model and are printed with a 50µm layer thickness. All these cubes are observed under the Profilometer (Figure 23) to find the microscale printing roughness.

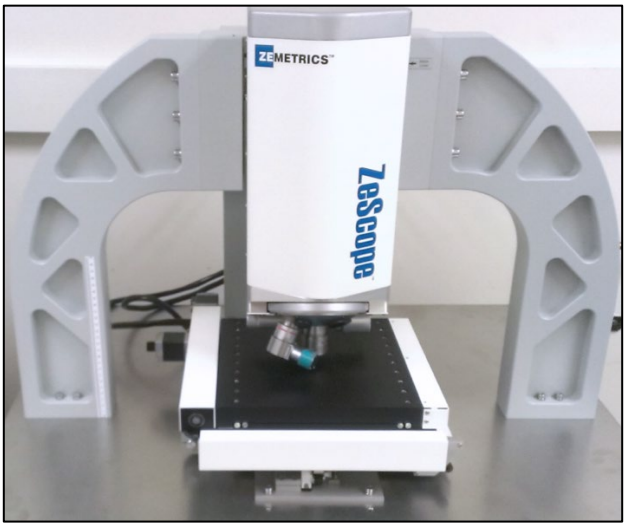

Figure 23: ZeScope Profilometer

CHAPTER 4

RESULTS AND DISCUSSION

4.1 Nanoparticles Distribution vs Dispersion Approach

To increase the surface roughness and structural strength of the superhydrophobic structures that are to be printed using e-VPP technique, nanofillers are added to the pure photopolymer resin. Due to the mechanical and electrical properties of the MWCNT, different weight mixtures of MWCNT are prepared using mixing techniques like Vortex and ultrasonic bath and magnetic stirred mixing techniques. The weight percentages of 0.5%, 1%, 1.5%, 2% and 2.5% of MWCNT are added to the pure photopolymer resin and are observed under a microscope for the rate of dispersion. The MWCNT mixture in all the above-mentioned concentrations needs to homogenous to prepare structures with best possible mechanical properties. And also, the homogenous mixtures are better at aligning under electric field which is the main objective of this whole project.

The photopolymer resin mixed with 1% MWCNT using Vortex and ultrasonic bath and Magnetic stirred methods are shown in Figure 24a and b respectively. The dispersed MWCNT can be clearly identified with the help of light coming out from the background. These two mixture techniques are observed for a duration of 60 min with a time interval of 15 min to notice the differences in the rate of dispersion. The weight percentages of MWCNT are mixed with vortex stirrer for 5 min and then placed inside the ultrasonic bath for the whole time. Parallelly, another mixture is placed on a magnetic stirring apparatus at a speed of 650 rpm. Both mixtures are compared using samples taken in the time intervals.

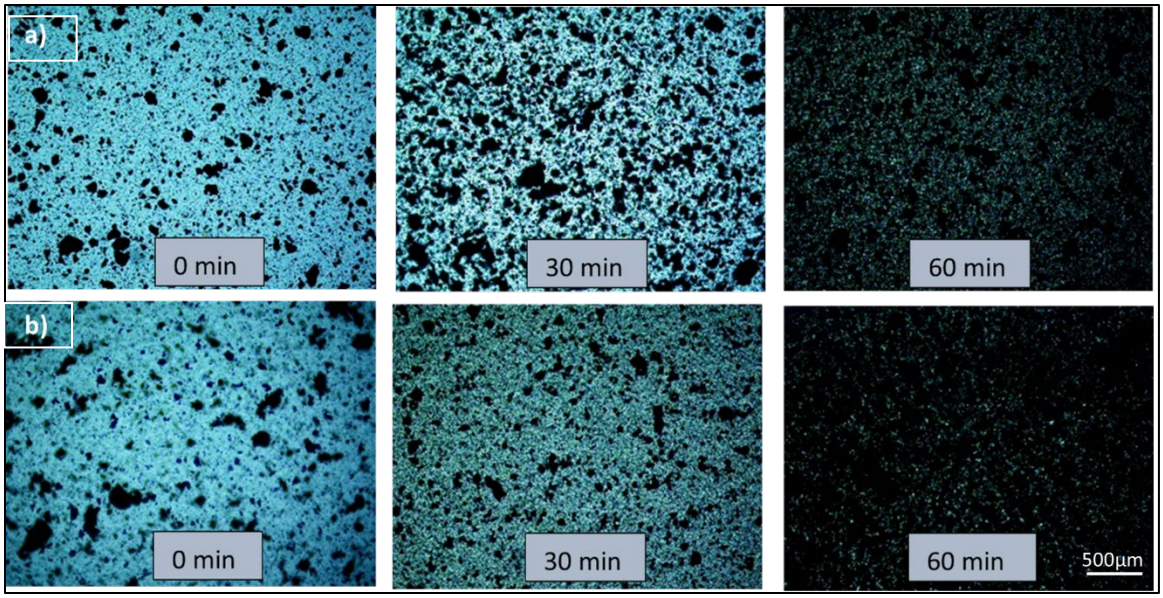

Figure 24: a) 1% MWCNT dispersion of Vortex Stirred Mixture for 0min, 30min and 60 min. b) 1% MWCNT dispersion of Magnetic Stirred Mixture for 0min, 30 min and 60min.

After mixing the resins with two different techniques, it is observed that the dispersion of magnetic stirred resin is much better compared to the vortex and ultrasonic bath mixture as the magnetic stirrer helps the MWCNT particles to mix homogenously and the mixture also stays homogenous for a long time. While working with the Magnetic Stirred mixture, the curing times are also better compared to the other technique. During these 15 min time intervals, all the concentrations of MWCNT, 0.5%, 1%, 1.5%, 2% and 2.5% shows significant dispersion rates. This can be further tested, and a mixing method can be selected by using the curing characteristics for these two Vortex and sonic bath and Magnetic stirred mixing techniques.

4.2 Curing Characterization

Curing Time is the amount of time needed for the photopolymerization of the polymer resin into solid material. The resin cures more quickly or more slowly depending

on the material added to it. MWCNT is added to the polymer resin, which reduces some of the energy that is emitted by UV light. When exposed to an electric field, the MWCNTs create microscale MWCNT strands that align in a horizontal line and block the projected UV light beam from starting the photopolymerization process of the photocurable resin. Due to the tightly packed bundles that are next to one another, this MWCNT accumulation, which is perpendicular to the 2D light beam, causes greater light dispersion. A relationship was developed to calculate the cure depth Cd of the photocurable resin using the light penetration, volume percentage, and total energy. The following equation, developed by Griffith and Halloran [27], could be used to predict the curing model of MWCNT-based resin during the e-VPP process:

$$C_d = \left(\frac{\eta_0}{\eta_P - \eta_0}\right)\frac{\lambda^2}{D}\ln\left(\frac{t}{t_c}\right)\frac{1}{\phi} \quad \text{[1]}$$

Where η_0 is the refractive index of the photocurable resin, η_P is the refractive index of the MWCNT, λ is the wavelength of light in nm, D is diameter of the MWCNT based bundle, t is the exposure time, t_C is the critical exposure time, and φ is the concentration of MWCNTs in the composite [54].

Different concentrations of the random and aligned MWCNT material, as well as pure photocurable polymer resin, were examined for their curing depth properties. The cure depth for both cases significantly decreased when the concentration of MWCNT was raised. For instance, pure polymer has a 0.50mm cure depth. The cure depths of this composite of these two mixtures are 0.295mm and 0.068mm, respectively, when 2.5% of MWCNT were uniformly dispersed throughout the liquid resin. Additionally, the cure depth decreased with increasing MWCNT concentration. A correlation between the

concentration of MWCNT, the curing depth and the exposure duration was shown in Figure 25.

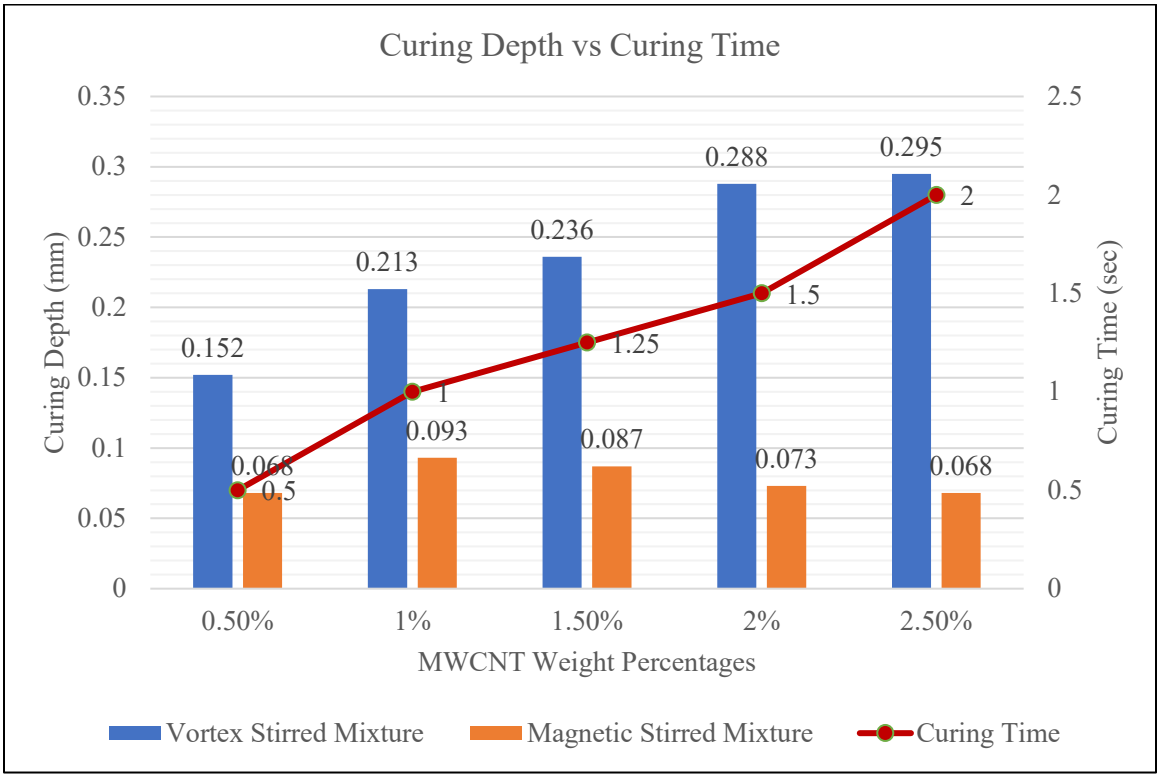

Figure 25: Curing depth vs Curing time for Vortex and Magnetic Stirred Mixture for 0.5%, 1%, 1.5%, 2% and 2.5% MWCNT Concentrations

After observing the curing times and depths for these two different mixture techniques, the magnetic stirred mixtures which already have better dispersion rate shows better curing depths. The magnetic stirred mixtures take 0.5sec,1sec and 1.25 sec to cure 0.068mm,0.093mm and 0.087 mm for 0.5%,1% and 1.5% respectively whereas the vortex and sonic bath takes 0.5sec,1sec and 1.25 sec to cure 0.152mm ,0.213mm and 0.236mm for the same. Which means that the vortex mixture is overcuring for the shortest printing times possible. Whereas the magnetic stirred mixtures are good at that

rate and the curing depth can be fixed for the respective mixtures. This further helps us to proceed this technique to prepare material to print with different concentrations.

4.3 MWCNT Alignment vs Electrical Field Strength Vs Dispersion Approach

4.3.1 MWCNT alignment vs electrical field

VPP 3D Printing do not need any electricity. But while aligning MWCNT under electric field, there is a need for Voltage source, and it need to be regulated. As MWCNT is highly conductive, it has the ability to change its directions at nanoscale. When it is introduced into AC Electric Field, it aligns in the direction of the field. Here, to align MWCNT under electric field, AC Voltage output is used at 1KV and 1.5KV. Under high voltage parameters, MWCNT tries to align more and more and then the small alignments observed can lead to form a thicker chain like structures in between the electrodes inside the resin. Some of the MWCNT can also be observed depositing at the electrodes. This leads to the separation of MWCNT from the resin which is not good for printing. Thus, MWCNT is observed under AC electric field for specific time intervals and the data is shown in Figure 26.

The time taken for the alignment of MWCNT in 0.5% mixture is gradually decreasing from 33 sec to 8 sec with increase in the AC Voltage from 0.5 KV to 2KV. This is because the high voltages activate the alignment of MWCNT present in the mixture. The same phenomenon can be observed in the rest of the mixtures as they are decreasing from 41 sec, 49 sec, 58 sec and 73 sec to 10 sec, 10 sec, 12 sec and 15 sec for 1%, 1.5%, 2% and 2.5% mixtures respectively.

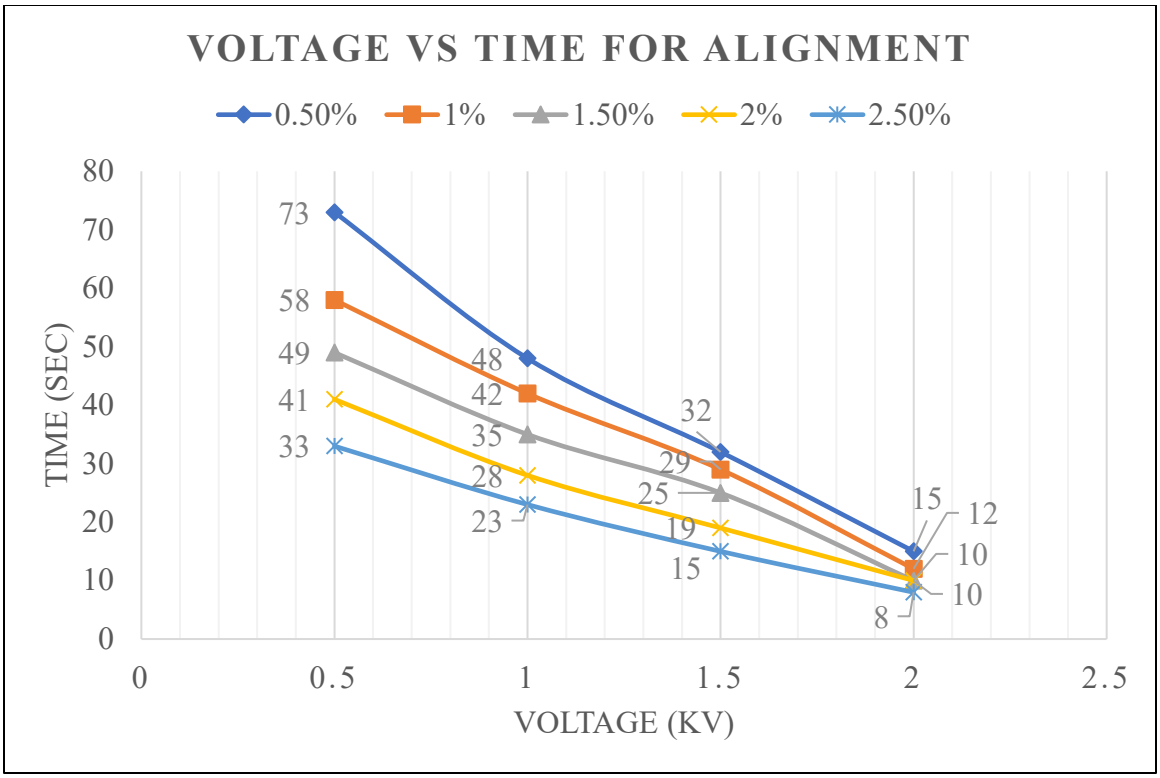

Figure 26: Voltage vs Time graph for alignment of mixtures of different MWCNT concentrations

On observing the variation in time taken for the MWCNT mixtures for the same voltage of 0.5KV, that is 33 sec for 0.5% to 73 sec for 2.5%, it can be said that the more the weight percentage of MWCNT present in the mixture, the more time it takes to align at low voltages, and it gradually decreases with increase in the AC voltage. That can be said at 2KV where 0.5% mixture takes 8sec and 2.5% takes 15 sec to align which is not a big difference.

4.3.2 MWCNT alignment vs Dispersion Approaches

The CNT alignment process has four steps. The application of an electric field in the first step allows a dipole moment to be created at the edges of the CNTs, which caused them to rotate to a different angle and aligned in the direction of electric field. In the second step, polarized CNTs are drawn to one another and come into direct contact,

producing an aggregate that mimics a chain. CNTs move toward and adhere to the negative electrode in the third step. CNTs discharge and assemble on the electrodes when they are sufficiently near to the electrode to transmit the charge. The electrode's attached CNTs serve as both principal absorbers of other CNTs and generators of strong fields. In the fourth step, further CNT bundles were joined to the first bundle after it had been connected to the negative electrode, and the aligned CNT network subsequently covered the space between the negative and positive electrodes. In fact, CNTs act as a conduit for the current to flow from the negative electrode to the positive electrode, and the phenomenon known as the relaxation mechanism occurs when the electric field is interrupted during the alignment process, causing the highly oriented network to disintegrate and the CNTs to return to their original locations.

In Figure 27 a, b, 1% MWCNTs mixture is observed under a microscope for alignment at 1KV and 2KV for a duration of 60 sec and 10 sec respectively. It is noted that the time difference for the alignment for these 2 different voltages is very high because the activation time for MWCNT under electric field gradually decreases with increase in voltage. And it is also observed that there is a formation of thick bundles that are overly aligned if the mixture is let under electric field for more duration. These thick bundles let the current flow through the resin creating a short circuit.

The thickness of MWCNT bundles formed with alignment changes accordingly with time and by its weight percentage. The aligned bundles for 1% mixture start from around 5-10µm during the beginning of alignment process at 30 sec and go all the way upto 90-100µm when the voltage is set at 1KV for 15 min.

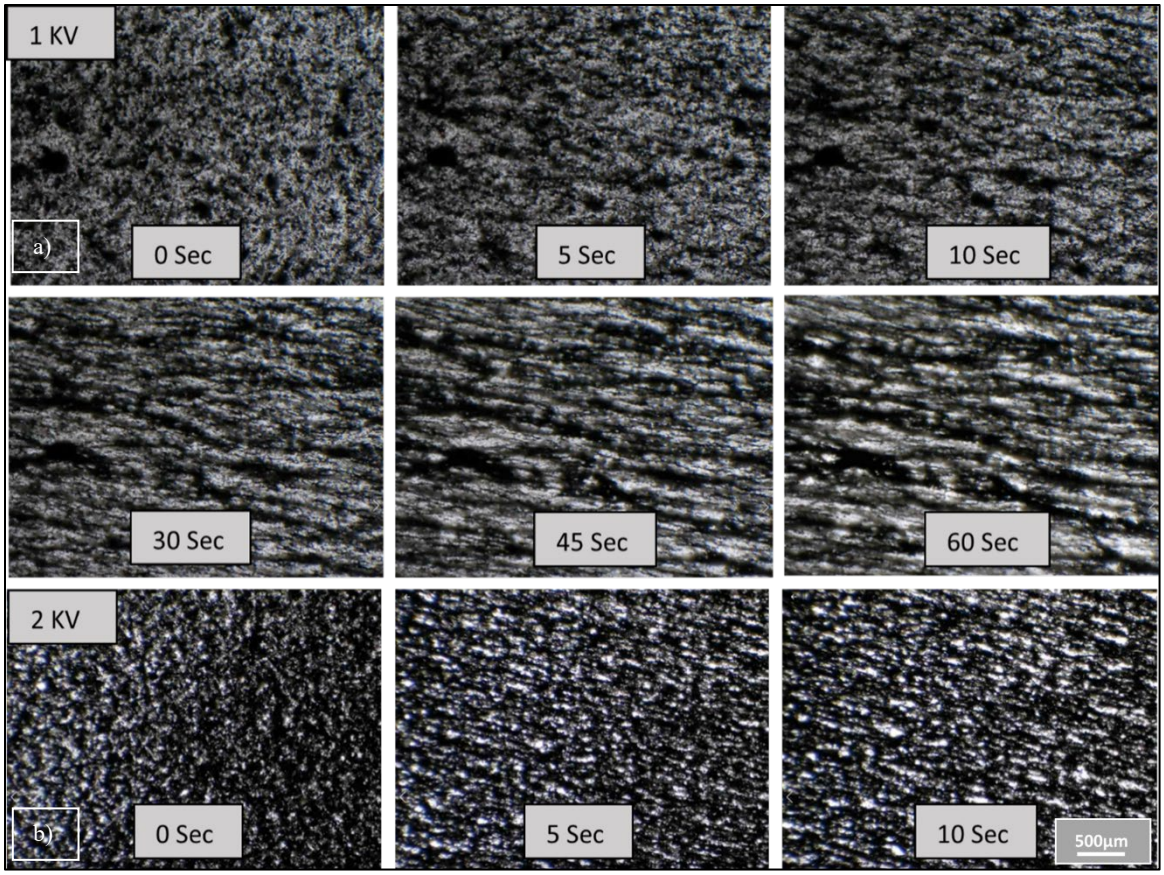

Figure 27: a) 1% MWCNT Mixture under 1KV for 0sec, 5sec, 10 sec, 30 sec, 45 sec and 60 sec. b) 1% MWCNT Mixture under 2KV for 0se, 5sec and 10 sec respectively.

The current starts flowing when this bundle gets thicker at 18 min and the Hipot Tester would shut down. So, to prevent this short circuit, the printing process should be finished before the thick bundle formation, or the voltage should be controlled so that it takes more time to form these bundles.

The flow of MWCNT inside the red resin under electricity for alignment changes with time. The time for alignment and the deposition of MWCNT at the electrodes depends on the percentage of MWCNT in the mixture, the voltage applied and also the time of application. So, the time for alignment should be observed carefully not to change the dispersion of MWCNT in the red resin which leads to changes in the structural

properties as well as the curing times. With increase in the mixture of MWCNT, the rate of alignment increases. And with increase in the AC voltage applied, the rate of alignment also increases. From the Figure 18 and 19, it is observed that the time required for higher percentages of MWCNT decreases rapidly with increasing voltage. 2.5% mixture takes 15 sec to align at 2KV, but it also increases the chances of these bundle formations faster and thicker compared to the other 2% and 1.5% mixtures at the same conditions because of the dispersion. Thus, MWCNT weight percentages, AC Voltage application, dispersion rate and the alignment of MWCNT are correlated to each other.

4.4 Roughness Evaluation vs MWCNT Concentration vs Electrical Field

A cube of 5mm (Figure 28) is designed and printed using E-VPP 3D printing with all the different mixtures of the resin, random and aligned with a layer thickness of 50µm to achieve a controlled layer thickness. All the mixtures of MWCNT are aligned under Electric field and are printed to get a set of samples to observe the microscale roughness of the printing that can be achieved with this form of 3D printing. This microscale roughness is an important factor in the Contact Angle measurement as the roughness changes the high and low CA of these structures and decide the hydrophobicity of a structure. All the mixtures of MWCNT 0%, 0.5%, 1%, 1.5%, 2% and 2.5% both random oriented and aligned mixtures are used to print the cube of length 5mm. All these samples are tested under a profilometer to observe the surface roughness as well as the print roughness that needs to be controlled. All these cubes are printed under electric field with a constant voltage of 1KV. This print roughness that is observed under the profilometer is considered as the microscale roughness that will be used in the manufacturing of superhydrophobic structures.

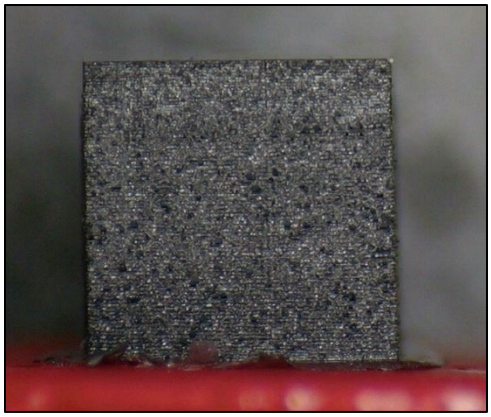

Figure 28: 1% Cube with Random alignment for roughness evaluation

When observed under profilometer each individual layer can be seen like grooves with convex and concave surfaces which tells us the roughness of each individual layer. Here we have three different studies just for the roughness measurement for both vortex and ultrasonic stirred mixture as well as the magnetic stirred mixture. They are random oriented, and then the aligned MWCNT roughness is tested in both horizontal orientation and vertical orientation i.e., the direction of electric field and the perpendicular direction to the electric field respectively.

From Figure 29 a, b we can see all the different trends that were caused by random orientation, horizontal and vertical sides of aligned MWCNT under 1KV for the mixtures of 0% 0.5%, 1%, 1.5%, 2% and 2.5% MWCNT mixtures. Different curing times and voltages are used four different mixtures of MWCNT to observe the roughness by keeping the curing depth constant at 50µm.For vortex mixture it is observed that the random MWCNT has high surface roughness at 2.5% that means the random orientation of MWCNT creates individual layers with high surface roughness at microscale. It is the same for magnetic state mixture as the surface roughness gradually increases from 0% to 2.5% MWCNT concentration. The roughness of 2.5% Vortex mixture is 12µm whereas

magnetic state mixture is 17µm. this explains that the roughness caused from printing these structures using magnetic stirred mixture is higher than the vortex mixture. This must be because of the rate of dispersion off the magnetic stirred mixture is better than the vortex and ultrasonic mixture.

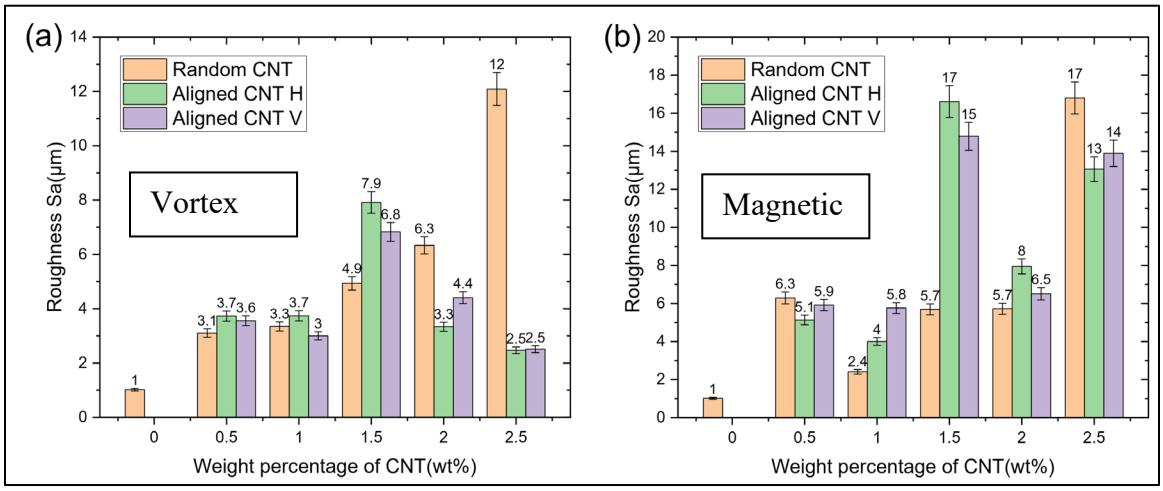

Figure 29: Roughness Measurements for a) Vortex Mixture and b) Magnetic Stirred Mixture

But on observing the horizontal and vertical sides of MWCNT alignment the trend is different from the random orientation. It can be because of the higher percentages of MWCNT present in the mixture causes more alignment which leads to a decrease in the surface roughness at micro scale in both vortex and magnetic stirred mixtures. For horizontal side of aligned MWCNT the roughness is 3.7 µm for 0.5% mixture and is increasing until 1.5% at 7.9 µm and then started decreasing for 2% and 2.5% mixture which is 3.3 µm and 2.5 µm for vortex mixture and the trend is almost same for the magnetic state mixture where the roughness is observed at 5.1 µm for 0.5%, 4 µm at 1% and it reached highest at 17 µm and then decreased to 8 µm at 2% and 13 µm for 2.5%. This nonlinear pattern explains that for aligned orientation there need not be more

MWCNT weight percentage needed for the mixture. It also explains that the roughness observed for the alignment is higher in magnetic stir mixture compared to the vortex state mixture.

In the aligned MWCNT, on the vertical side, the roughness measurements observed are almost similar to the horizontal side for both vortex and magnetic stirred mixtures. it starts from 3.6 µm 3 µm and reaches 6.8 µm and then decreases to 4.4 µm and 2.5 µm for 0.5%, 1%, 1.5%, 2% add 2.5% respectively this trend is almost similar to the horizontal alignment. Now the magnetic stirred mixture is also similar, but the roughness is a bit higher than the vortex mixture and starts at 5.9 µm for 0.5% ,5.8 µm for 1% and reaches to 15 µm for 1.5% and then decreases to 6.5 µm for 2% and finally 14 µm for 2.5%. The trends that are observed for both horizontal and vertical mixtures of MWCNT alignment for both vortex and ultrasonic mixture and magnetic stirred mixture are similar and are reaching the peak roughness at 1.5% compared to the random MWCNT alignment which is reaching the peak toughness at 2.5%. Thus, the rate of dispersion, the amount of MWCNT weight percentage added to the resin alters the roughness of the print for each individual layer when aligned under electric field. The correlation between

4.5 Mechanical Simulation

By adding gravity to the droplets, it was possible to mimic how water droplets would compress on a 3D-printed eggbeater structure. The model was designed in SolidWorks and simulated in COMSOL Multiphysics (Figure 22). The modulus is set at 1.95 GPa, 2.13 GPa, and 2.29 GPa for Red Resin, 0.5% MWCNT mixture, and aligned mixture, respectively. The water droplet is assumed to be stationary, and the applied force

is the gravity on the droplets to study the deformation of eggbeater arrays. In order to observe the deformation of eggbeater arrays in various directions, a side force was also applied.

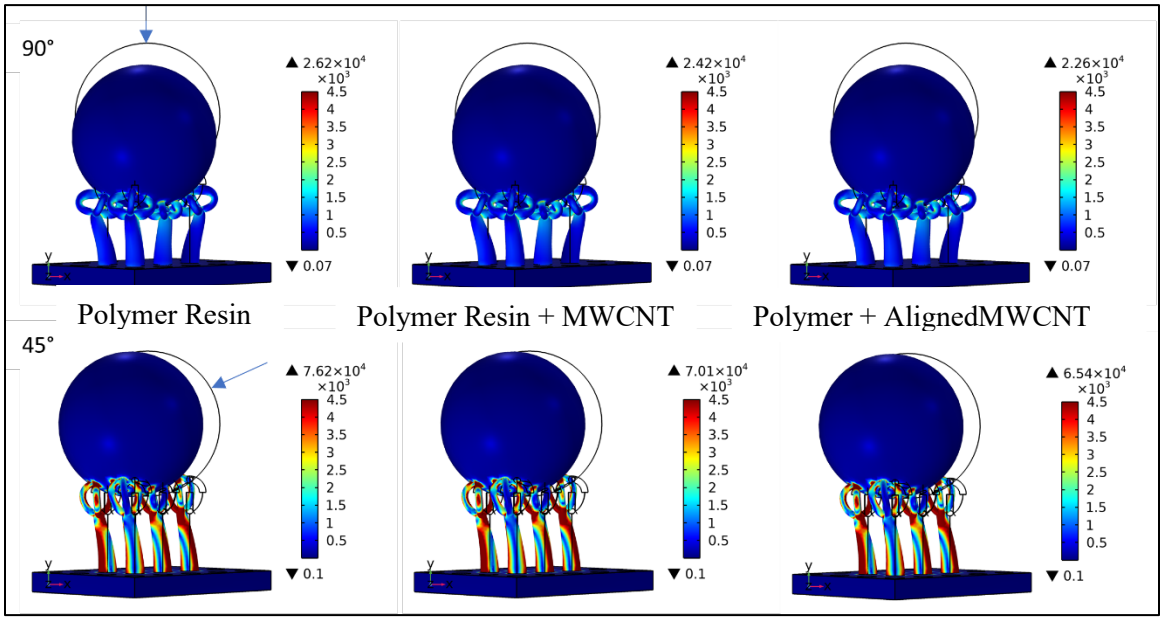

Figure 30: COMSOL Simulations on eggbeater structures at 90°and 45° for Red, random and aligned MWCNT Mixtures.

As show in Figure 30, the red resin made structure has stresses of 26.2 MPa which is the highest for all the vertical drop simulations. This is because the structural strength of the structure made using pure photopolymer is low compared to the MWCNT mixture made structures. The modulus increases with the help of these nanofillers, and the stresses induced is reduced to 24.2 MPa. And then for the aligned mixture, the stresses are even more reduced to 22.6 MPa which describes significant increase in the structural strength of the eggbeater structures under same loading conditions.

Like the vertical loads, the stresses induced in 45° angle are gradually decreasing from 76.2 MPa, 70.1 MPa to 65.4 MPa for Polymer resin, MWCNT random and aligned

orientation. The side force applied induces more stresses on these structures compared to the vertical drop as shown in Figure 31. This is because the structures created using this e-VPP technique are structurally strong in the vertical direction, that means they can absorb more compressive forces compared to the tensile forces. These structures are more brittle in nature and are easily destroyed if small forces are applied in the horizontal direction or from an angled direction compared to the vertical direction.

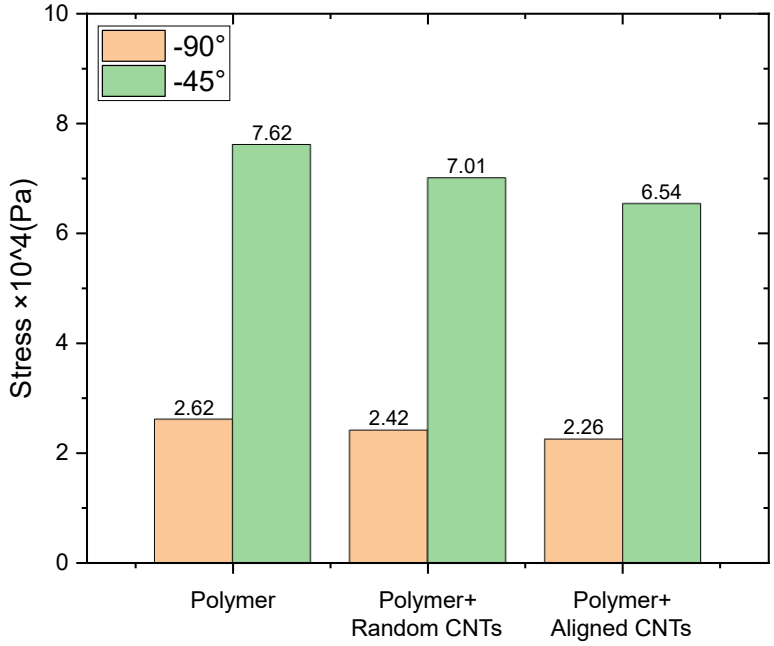

Figure 31: COMSOL Simulation of Stresses induced for Polymer resin, 1% MWCNT random and aligned mixtures when water droplet is dropped from 90° and 45°

The results suggest that under a load applied in the 90° direction, the stress is centered on the tips of the eggbeater arrays whereas the 45° direction, they are involving most of the body which is brittle in nature. The strain is concentrated across the eggbeater arms when the stress is altered in the YZ plane by 45 degrees. It is observed that when number of arms increases and the load remains constant, the strain on the tips decreases.

According to the results, the 3D-printed eggbeater hairs act as soft springs in the same way as the eggbeater-shaped trichomes on the leaves of Salvinia Molesta do.

4.6 Contact Angle vs Geometric Design of Eggbeater-Shaped Structures

A syringe needle was used to deliver a water droplet to the surface to evaluate the structure's super-hydrophobicity. The droplet maintains its circular form on the surface. An optical microscope was used to capture a side view photo of the produced droplet, which was then imported into "Image J Software" for Contact *Angle measurement.* The contact angle increases as the distance between the eggbeater structures widens. The increased surface area between the eggbeater tip and the water droplet is responsible for this. The eggbeater structure with more distance, on the other hand, does not have any hydrophobicity. This is due to the size of the water droplet that is dropped on these structures and the simultaneous distribution of it on each arm.

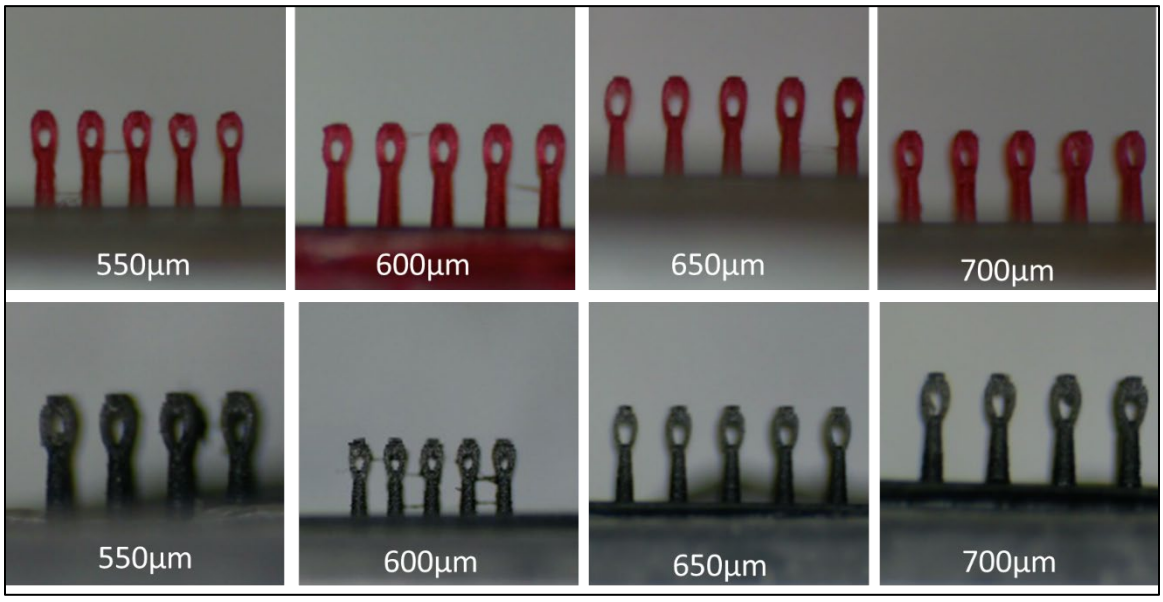

Figure 32: Printed Eggbeater Structures with Red Resin and 0.5% MWCNT

The eggbeater arrays function best when there is a gap of 500 μm between them (Figure 32), taking into account the structures' super hydrophobicity and strength. Additionally, zero velocity conditions are occurring at the surface of the wetted region due to the hydrophilic tip of the eggbeater arrays. As a result, the air-water contact will stabilize at a certain level above the hairs. To minimize the contact area, the arms are twisted together at the terminal ends. In order to effectively stabilize the air-water interface, the energy needed for the water to enter the space between the hairs must be increased. In order to provide as much surface per height difference as feasible, the hairs are divided into four arms. The eggbeater hairs' elastic qualities are useful in preventing the rupture of the air-water interface contact.

For the eggbeater structure in contact with water, there are four main types of contact regimes. W–W, CB–CB, W_M–CB_m, CBM–W_m, W is for Wenzel, CB for Cassie-Baxter, and the subscripts "M" and "m" stand for "Macro" and "Micro," respectively. [19] The contact angle for the CB-CB state is determined by

$$\cos(\theta_{CB}^{CB}) = f_{SL}\cos(\theta) - f_{LA} \quad [2]$$

Here, f_{SL} and f_{LA} stand for, respectively, the proportion of solid-liquid and liquid-air interfaces.

Regarding the mixed CB_M-W_m state (lower/macro-Cassie-Baxter and upper/micro-Wenzel), an air layer is trapped between the substrate and the base of the hairs' heads, and a water droplet is pinned on top of the eggbeater arms. Here we can anticipate the contact angle by

$$cos(\theta_{CB}^{CB}) = Rf_{SL}\,cos(\theta) - f_{LA} \quad [3]$$

The simplest method for understanding hydrophobicity (Figure 33) is to examine at the angle at which water contacts different surfaces. A separation line between the water, the substrate, and the air appears when a little drop of water is put on a substance.

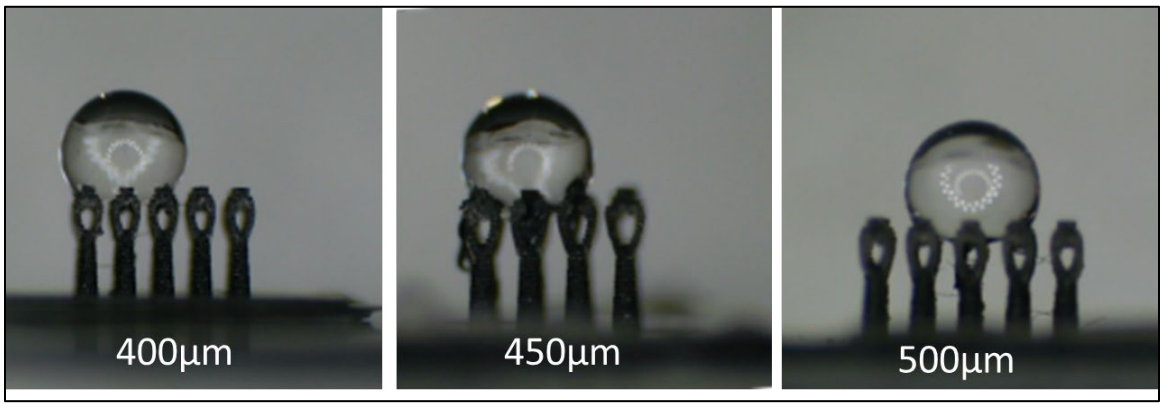

Figure 33: Eggbeaters showing superhydrophobic properties for water droplet

Although this concept of hydrophobic has been questioned, the standard definition of hydrophobicity is 90 degrees. It is clear from the contact angle definition of hydrophobicity that hydrophobic solids are typically "low-surface-energy" solids that interact primarily via dispersive interactions. Significant hydrogen bonds form between water molecules. The reduction of the area of contact and the resulting increased contact angle are caused by the partial loss of hydrogen bonding of water molecules in contact with a hydrophobic material, which does not perform hydrogen bonding.

The contact angles are going from 110.21° to 115.984° and 118.613° for 400µm, 450µm and 500µm respectively according to Figure 34. And then it is decreasing for the 550 µm and 600µm at 93.651° and 91.53° for the pure resin as the eggbeater structure could not hold the drop on its heads. This pattern is same for the 0.5% MWCNT mixture. It is reaching peak at 500µm with a CA of 127.362° and for other gaps of 400µm,

450µm, 550µm and 600µm, the contact angles obtained are 123.751°, 125.673°, 96.452° and 92.342° respectively. This explains that the contact angle reaches its peak at 500µm gap between each individual eggbeater for both resins. So further experiments with 1%, 1.5%, 2% and 2.5% MWCNT mixtures can be tested with the same geometry. This can help the random and aligned MWCNT mixtures to reach superhydrophobicity. The contact angles observed for the 500 µm are higher for Red Resin and also the 0.5% MWCNT mixture. Though they are not superhydrophobic, there is a hydrophobic behavior in these two models. So for further tests and prints with 1%, 1.5%, 2% and 2.5% concentrations of MWCNT, 500µm gap is selected and are tested for the same.

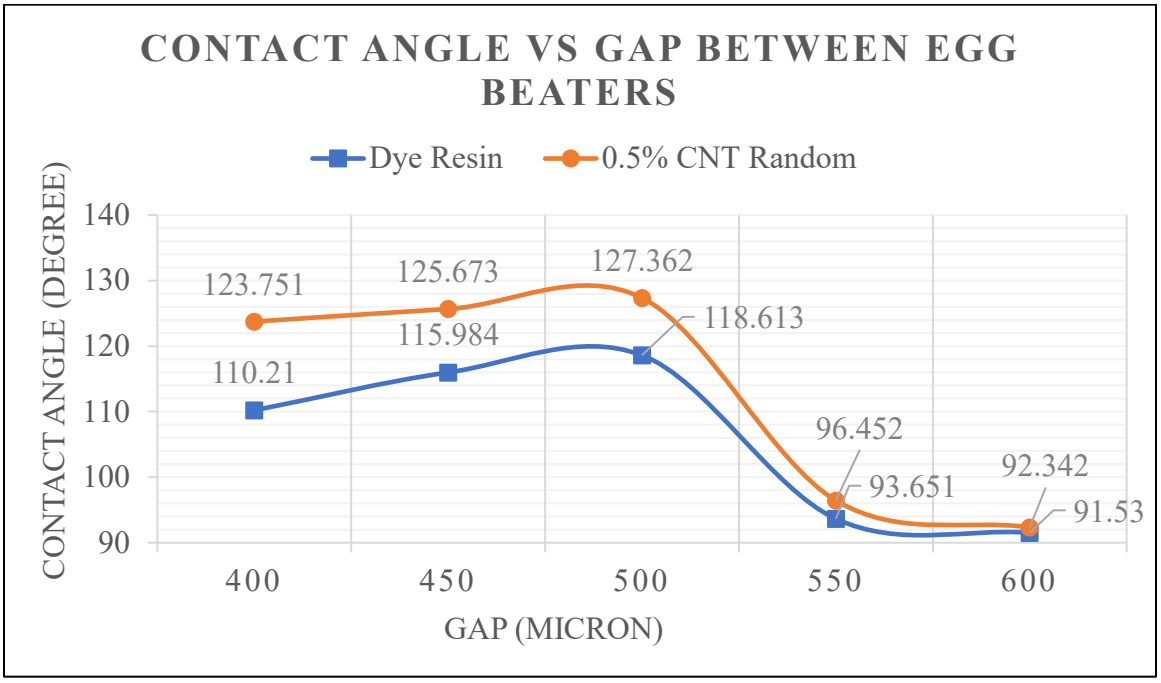

Figure 34: Contact Angles observed for Red Resin and 0.5% MWCNT with different gaps

4.7 Contact Angle vs MWCNT Concentration vs Electrical Field

The mixtures for different concentrations of MWCNT from 0.5% to 2.5% are made using Magnetic Stirring method and the eggbeater structures are made using these

different concentrations. The contact angles are measured from the images taken while dispensing water droplets of made when the water droplets of 5-7.5µL are placed above these structures. Then the measured contact angles are observed and are shown in Figure 35. If the CA from Red Resin is also compared to the same, there is a huge difference in the observed CA with MWCNT present in it. That states that MWCNT is improving the surface roughness of these structures and helping improve their superhydrophobicity.

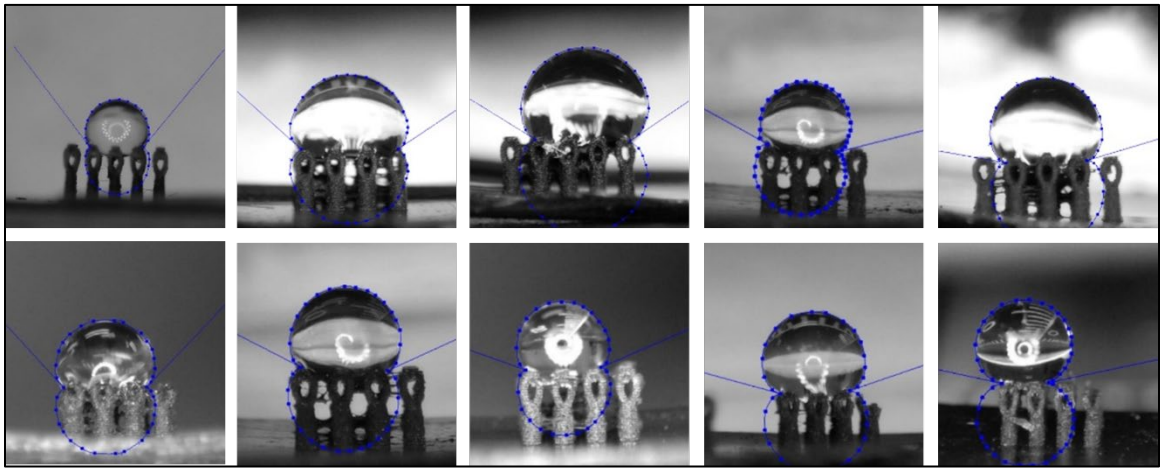

Figure 35: Contact Angle for different mixtures of MWCNT with and without electricity.

The Contact Angle for the Random and Aligned mixtures of MWCNT are observed using ImageJ software. The maximum CA can be observed for the 2.5% MWCNT Aligned mixture at 169.492° and the next highest is observed at 165.263° for the Random MWCNT mixture. These results states that the alignment of MWCNT could improve the Contact Angle of these structures which increases the superhydrophobicity of these structures.

The contact angles for random and aligned MWCNT for are shown in Figure 36. The pure red resin and 0.5% MWCNT random mixture with 500µm gap between the individual eggbeaters are selected as they have the highest contact angle of 118.613° and

127.362° respectively. Then the contact angle for random oriented MWCNT mixtures, it is increasing from 1% to 2.5% gradually with 146.414°, 149.94°, 159.451° and 165.263° for 1%, 1.5%, 2% and 2.5% respectively. This shows that these random MWCNT mixtures have superhydrophobic properties. These MWCNT mixtures acts as nanofillers to increase the roughness at micro-scale and improving the contact angle and superhydrophobic properties.

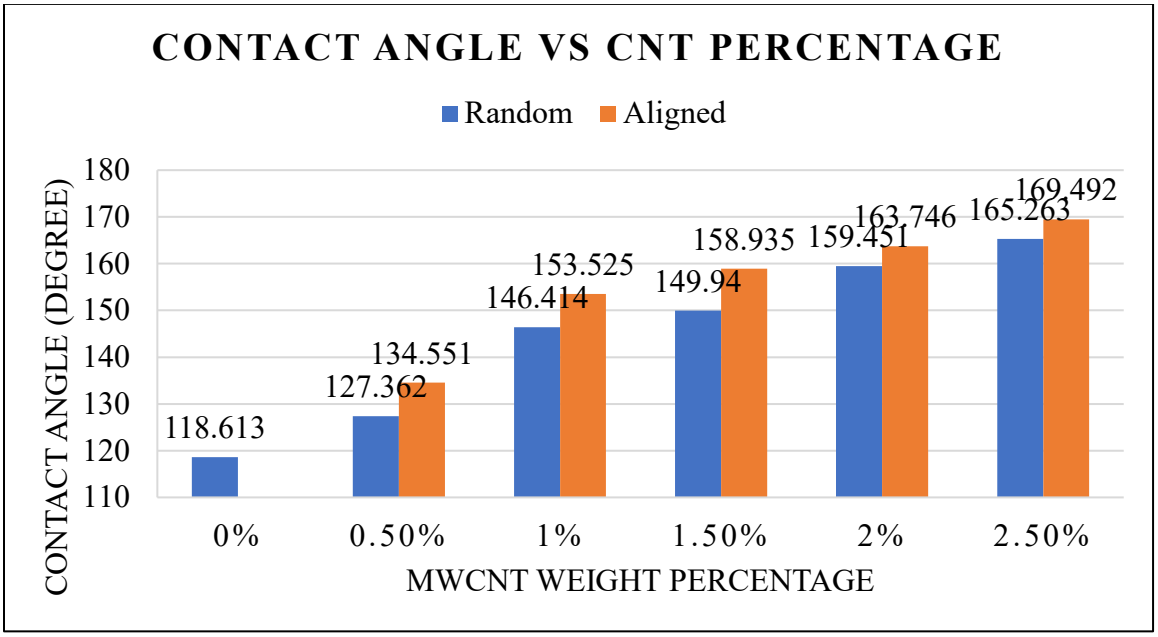

Figure 36: Contact Angle vs different mixtures of MWCNT graph with 500µm gap with and without Electricity for alignment.

Now, the aligned mixtures of MWCNT are showing much better contact angles at 134.551°, 153.525°,158.935° and 163.746° for 0.5%, 1%, 1.5% and 2% respectively. The highest contact angle observed for any of these structures is with 2.5% MWCNT mixture with 169.492°. On comparing the contact angles of random mixtures of MWCNT and aligned mixtures, we can state that the alignment of MWCNT under electric field improves the superhydrophobic properties of these eggbeater structures by a small factor.

4.8 Attaching Force Vs MWCNT Concentration Vs Electrical Field On/Off States

The profile may be fitted with an elliptical function as indicated in Equation 4, y(x), with fitting parameters a, b, and c. From Equation (5), the surface area of the meniscus may be calculated, together with the energy necessary to form the meniscus (6) and the maximum pulling force on the eggbeater (7) that corresponds to the water adhesion force of the eggbeater tip. Based on the picture before the meniscus ruptures, an elliptic function may be fitted to the meniscus' profile:

$$y(x) = -\frac{b}{a}\sqrt{a^2 - \left(x - a - \frac{c}{2}\right)^2} + b \qquad [4]$$

Having the parameters, a, b, and c. When the function y(x) is rotated around the y-axis, the rotationally symmetric form of the meniscus in three dimensions can be represented, allowing the surface area of the water meniscus to be calculated as:

$$A = 2\pi \int_0^b x(y)\sqrt{1 + \left(x'(y)\right)^2}\, dy \qquad [5]$$

Calculations were performed using MATLAB. Minimum energy necessary to generate the meniscus, starting with the initially flat surface prior to capillary contact, is:

$$W = A\sigma + \pi\left(\frac{c}{2}\right)^2 \sigma^* - \pi\left(a + \frac{c}{2}\right)^2 \sigma \qquad [6]$$

It comprises of the surface energy of the meniscus plus the interface energy of the tip-water contact region minus the surface energy of the initial flat air-water interface prior to capillary contact development. Here, σ = 0.07275 N/m is the water's surface tension, and σ^* is the contact area's interface tension. Despite the fact that σ^*'s value is unknown; it is not necessary for subsequent computations (7). The force pushing at the eggbeater's tip is equivalent to its water adhesion force and may be calculated as follows:

$$F = \frac{\partial W}{\partial b} = \frac{\partial A}{\partial b} * \sigma \qquad [7]$$

Two orders of magnitude less than the contribution of the expanding liquid surface were the meniscus weight force. This is calculable for the liquid volume inside the meniscus, as stated in

$$V = 2\pi[\int_0^{c/2} x * b dx + \int_{c/2}^{a+c/2} x * y(x) dx] \quad \text{[8]}$$

and hence $F_G = \rho V g$ is the weight force, where is the liquid's density and g are the acceleration of gravity. Typically, the weight force of the water inside the meniscus contributes negligibly to the force pushing at the tip in contact with the water.

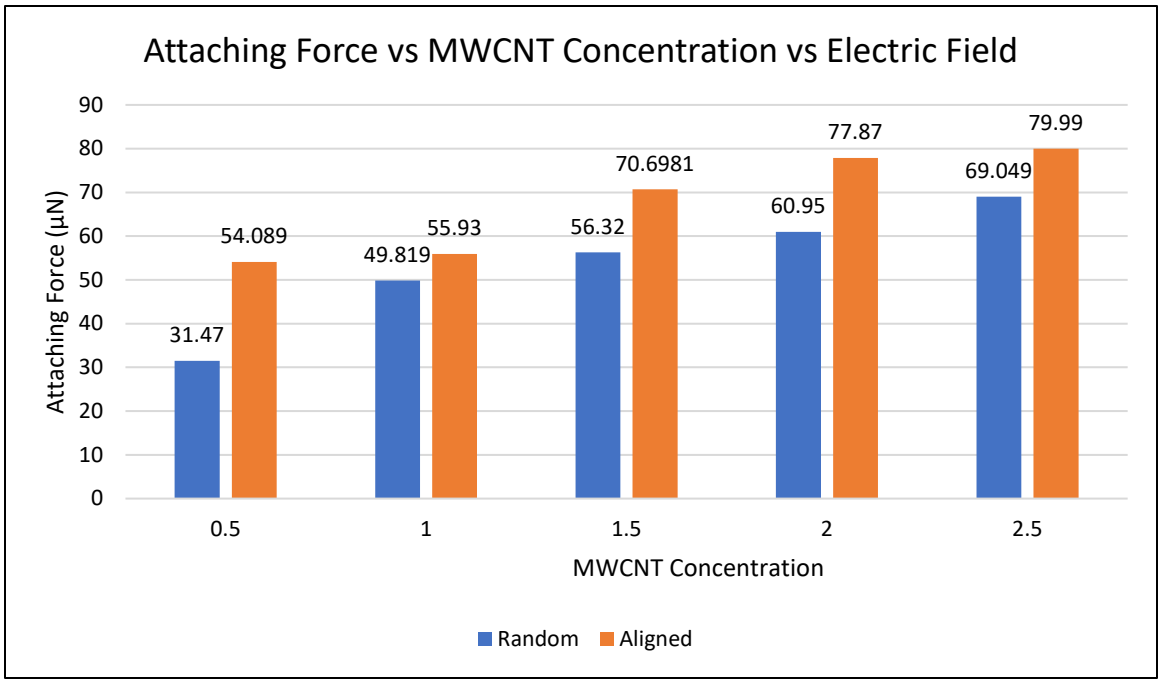

Figure 37: Attaching Force vs MWCNT Concentration with and without Electric Field.

As shown in Figure 37, the maximum attaching forces are observed for the aligned MWCNT structures. And the maximum force observe is for 2.5% MWCNT mixture which is the maximum MWCNT weight percentage aligned in this experiment. The results demonstrated that the adhesive force increased from low (31 N) to high (80

N) with an increase in the percentage of MWCNT added to the resin. This growth is related to the alteration of the roughness in the microstructure scale and shape, which creates various sticky regions for water droplets on the surface. The results show that the printed eggbeater structure using the e-VPP 3D printing technique has a controlled adhesive force for both the Random and aligned MWCNT mixtures but the adhesive forces observed for the Aligned MWCNT are higher than the other by atleast 5-20μm in different concentrations.

CHAPTER 5

CONCLUSION AND FUTURE WORK

5.1 Summary

The rough nanoscale hierarchical surface produces air pockets, significantly reducing the solid-liquid interaction. The smaller solid-liquid contact area makes the surface hydrophobic because it enables water droplets to virtually perfectly spherical and easily slide off it. The wetting properties of the printed structured surface samples were tested in this study, and they were compared with aligned mixtures of MWCNT surface samples printed with the same process parameters but made of different material compositions. A surface's wetting behavior is primarily controlled by its chemical composition, micro and nanoscale roughness, and surface geometry.

As a result of this study, one unique additive manufacturing technique has been presented forward to develop hierarchical superhydrophobic structures with multi-scale roughness. Analysis and experimental validation have been done on the relationship between material qualities, manufacturing process parameters, and surface structure and geometry parameters. Analytical models and experimental data were used to evaluate the impact of manufacturing parameters and material characteristics on printed surface structure geometries, including aligned MWCNT structures and printed eggbeater structures. Wetting characteristics of the hierarchical surface structures were also examined along with the mechanical properties like attaching forces. The study supports the feasibility of creating multi-scale hierarchical surface structures inspired by biological systems by aligning MWCNT under an electric field, which has a number of potential real-world applications.

5.2 Future Work

Experimental results shows that the use of MWCNT increases the superhydrophobic properties of these structures at a high rate compared to the normal pure resins. Alignment of MWCNT could also help develop the other properties in these biomimetic structures inspired from Salvinia like Air-retention. The Super-hydrophobic air-retaining properties are observed from Salvinia to prevent wetting and submersion. The superhydrophobic air-retaining hairs feature hydrophilic tips at their ends, which pin the air-water contact. In one instance, the contribution of this pinning effect to air-layer stability under pressure variations is investigated using theoretical and experimental methods. The adhesion forces of individual hairs to the water surface are calculated using the capillary adhesion methods. This air retention properties also allow these superhydrophobic hierarchical structures for multiple applications like droplet control, microdroplet non-loss transportation and also oil-water separation. There are several studies that are using pure resins to improve these particular properties for any kind of biomimetic hierarchical structures. But the above mentioned MWCNT alignment E-VPP 3D Printing can bring multiple new results that can be used for different applications in the future of 3D Printing as well as Biomimicry.

REFERENCES

[1] X. Gao, L. Jiang, Nature 2004, 432, 36.

[2] Gao, W., Zhang, Y., Ramanujan, D., Ramani, K., Chen, Y., Williams, C.B., Wang, C.C., Shin, Y.C., Zhang, S. and Zavattieri, P.D., 2015. The status, challenges, and future of additive manufacturing in engineering. *Computer-Aided Design*, *69*, pp.65-89.

[2] K. Autumn, Y. A. Liang, S. T. Hsieh, W. Zesch, W. P. Chan, T. W. Kenny, R. Fearing, R. J. Full, Nature 2000, 405, 681.

[3 Li, X. and Chen, Y., 2018

[4] K. Koch, B. Bhushan, W. Barthlott, Prog. Mater. Sci. 2009, 54, 137.

[5] X. Yao, Y. Song, L. Jiang, Adv. Mater. 2011, 23, 719.

[6] R. Blossey, Nat. Mater. 2003, 2, 301.

[7] A. Lafuma, D. Quéré, Nat. Mater. 2003, 2, 457.

[8] M. J. Hancock, K. Sekeroglu, M. C. Demirel, Adv. Funct. Mater. 2012, 22, 2223.

[9] Y. Zhu, J. Zhang, Y. Zheng, Z. Huang, L. Feng, L. Jiang, Adv. Funct. Mater. 2006, 16, 568.

[10] J. Yuan, X. Liu, O. Akbulut, J. Hu, S. L. Suib, J. Kong, F. Stellacci, Nat. Nanotechnol. 2008, 3, 332.

[11] M. Jin, J. Wang, X. Yao, M. Liao, Y. Zhao, L. Jiang, Adv. Mater. 2011, 23, 2861.

[12] Z. Xue, S. Wang, L. Lin, L. Chen, M. Liu, L. Feng, L. Jiang, Adv. Mater. 2011, 23, 4270.

[13] W. L. Min, B. Jiang, P. Jiang, Adv. Mater. 2008, 20, 3914.

[14] M. Jin, X. Feng, L. Feng, T. Sun, J. Zhai, T. Li, L. Jiang, Adv. Mater. 2005, 1, 1977.

[15] X. J. Feng, L. Jiang, Adv. Mater. 2006, 18, 3063.

[16] D. Quéré, Nat. Mater. 2002, 1, 14. [17] W. Barthlott, T. Schimmel, S. Wiersch, K. Koch, M. Brede, M. Barczewski, S. Walheim, A. Weis, A. Kaltenmaier, A. Leder, H. F. Bohn, Adv. Mater. 2010, 22, 2325.

[18] A. Solga, Z. Cerman, B.F. Striffler, M. Spaeth, W. Barthlott, Bioinspiration Biomimetics 2007, 2, S126. [19] O. Tricinci, T. Terencio, B. Mazzolai, N. M. Pugno, F. Greco, V. Mattoli, ACS Appl. Mater. Interfaces 2015, 7, 25560.

[20] N. Zhao, Q. Xie, X. Kuang, S. Wang, Y. Li, X. Lu, S. Tan, J. Shen, X. Zhang, Y. Zhang, J. Xu, C. C. Han, Adv. Funct. Mater. 2007, 17, 2739.

[21] Y. Lai, X. Gao, H. Zhuang, J. Huang, C. Lin, L. Jiang, Adv. Mater. 2009, 21, 3799.

[22] F.D. Nicola, P. Castrucci, M. Scarselli, F. Nanni, I. Cacciotti, M.D. Crescenzi, Nanotechnology 2015, 26, 145701.

[23] Y. Yang, Z. Chen, X. Song, B. Zhu, T. Hsiai, P.I. Wu, R. Xiong, J. Shi, Y. Chen, Q. Zhou, K.K. Shung, Nano Energy 2016, 22, 414.

[24] Yan, C., Jiang, P., Jia, X. and Wang, X., 2020.

[25] Tricinci, O., Terencio, T., Mazzolai, B., Pugno, N.M., Greco, F. and Mattoli, V., 2015.

[26] J. E. Mates, I. S. Bayer, J. M. Palumbo, P. J. Carroll, C. M. Megaridis, Nat. Commun. 2015, 6, 8874.

[27] Joyee, E. B., Lu, L., and Pan, Y., 2019,

[28] J. Friedrich, C. Seidel, R. Ebner, L. A. Kunz-Schughart, Nat. Protoc. 2009, 4, 309.

[29] S. Lee, B. Kim, S. H. Kim, E. Kim, J.H. Jang, Adv. Funct. Mater. 2017, 27, 1702310.

[30] L. Feng, S. Li, Y. Li, H. Li, L. Zhang, J. Zhai, Y. Song, B. Liu, L. Jiang, D. Zhu, Adv. Mater. 2002, 14, 1857. [31] B. Bhushan, E. K. Her, Langmuir 2010, 26, 8207.

[32] J. Yuan, X. Liu, O. Akbulut, J. Hu, S. L. Suib, J. Kong, F. Stellacci, Nat. Nanotechnol. 2008, 3, 332.

[33] X. Hong, X. F. Gao, L. Jiang, J. Am. Chem. Soc. 2007, 129, 1478. [34] D. Quéré, Annu. Rev. Mater. Res. 2008, 38, 71.

[35] Z. Cheng, M. Du, H. Lai, N. Zhang, K. Sun, Nanoscale 2013, 5, 2776.

[36] X. Tang, P. Zhu, Y. Tian, X. Zhou, T. Kong, L. Wang, Nat. Commun. 2017, 8, 14831.

[37] J. Lv, Z. Gong, Z. He, J. Yang, Y. Chen, C. Tang, Y. Liu, M. Fan, W. M. Lau, J. Mater. Chem. A 2017, 5, 12435.

[38] Y. Chen, C. Zhou, J. Lao, Rapid Prototyping J. 2011, 17, 218.

[39] X. Zhao, Y. Pan, C. Zhou, Y. Chen, C. C. L. Wang, J. Manuf. Processes 2013, 15, 432

[40] H. Mao, C. Zhou, Y. Chen, J. Manuf. Processes 2016, 24, 406.

[41] Cai, Y., Xu, Z., Wang, H., Lau, K.H.A., Ding, F., Sun, J., Qin, Y. and Luo, X., 2019.

[42] Yang, X., Liu, X., Li, J., Huang, S., Song, J. and Xu, W., 2015.

[43] Su, F. and Yao, K., 2014.

[44] Shen, L., Fan, M., Qiu, M., Jiang, W., & Wang, Z. (2019).

[45] Wang, X., Cai, X., Guo, Q., Zhang, T., Kobe, B. and Yang, J., 2013.

[46] Dong, Z., Vuckovac, M., Cui, W., Zhou, Q., Ras, R.H. and Levkin, P.A., 2021.

[47] Haghanifar, S., Galante, A.J., Zarei, M., Chen, J., Tan, S. and Leu, P.W., 2022.

[48] Wang, D., Chen, D. and Chen, Z., 2020.

[49] Tricinci, O., Terencio, T., Mazzolai, B., Pugno, N.M., Greco, F. and Mattoli, V., 2015.

[50] Kim, M., Yoo, S., Jeong, H.E. and Kwak, M.K., 2022.

[51] Xiang, Y., Huang, S., Huang, T.Y., Dong, A., Cao, D., Li, H., Xue, Y., Lv, P. and Duan, H., 2020.

[52] Yang, Y., Li, X., Zheng, X., Chen, Z., Zhou, Q. and Chen, Y., 2018.

[53] Li, X., Yang, Y. and Chen, Y., 2017.

[54] Joralmon, D., Amonoo, E., Zhu, Y. and Li, X., 2022.

[55] Zhu, Y., Tang, T., Zhao, S., Joralmon, D., Poit, Z., Ahire, B., Keshav, S., Raje, A.R., Blair, J., Zhang, Z. and Li, X., 2022.